HHS Public Access

Author manuscript

Cerebellum. Author manuscript; available in PMC 2016 June 01.

Published in final edited form as:

Cerebellum. 2015 June ; 14(3): 292–307. doi:10.1007/s12311-014-0640-x.

The spontaneous ataxic mouse mutant *tippy* is characterized by a novel Purkinje cell morphogenesis and degeneration phenotype

Evelyn K. Shih[1], **Gabriella Sekerková**[2], **Gen Ohtsuki**[3], **Kimberly A. Aldinger**[4], **Victor V. Chizhikov**[5], **Christian Hansel**[6], **Enrico Mugnaini**[7], and **Kathleen J. Millen**[4,8,*]

[1]Division of Neurology, The Children's Hospital of Philadelphia, Philadelphia, Pennsylvania 10194

[2]Department of Physiology, Northwestern University Feinberg School of Medicine, Chicago, IL, 60611

[3]Department of Molecular Physiology, Kyushu University, Kyushu University, Graduate School of Medical Sciences, Higashi-ku, Fukuoka 812-8582, Japan

[4]Center for Integrative Brain Research, Seattle Children's Research Institute, Seattle, Washington, 98101

[5]Department of Anatomy and Neurobiology, The University of Tennessee Health Science Center, Memphis, Tennessee, 38163

[6]Department of Neurobiology, The University of Chicago, Chicago, Illinois 60637

[7]Department of Cellular and Molecular Biology, Feinberg School of Medicine and Hugh Knowles Center, Northwestern University, Chicago, Illinois, 60611

[8]The University of Washington Department of Pediatrics, Seattle, Washington, 98101

Abstract

This study represents the first detailed analysis of the spontaneous neurological mouse mutant, *tippy*, uncovering its unique cerebellar phenotype. Homozygous *tippy* mutant mice are small, ataxic and die around weaning. Although the cerebellum shows grossly normal foliation, *tippy* mutants display a complex cerebellar Purkinje cell phenotype consisting of abnormal dendritic branching with immature spine features and patchy, non-apoptotic cell death that is associated with widespread dystrophy and degeneration of the Purkinje cell axons throughout the white matter, the cerebellar nuclei and the vestibular nuclei. Moderate anatomical abnormalities of climbing fiber innervation of *tippy* mutant Purkinje cells were not associated with changes in climbing fiber-EPSC amplitudes. However, decreased ESPC amplitudes were observed in response to parallel fiber stimulation and correlated well with anatomical evidence for patchy dark cell degeneration of Purkinje cell dendrites in the molecular layer. The data suggest that the Purkinje neurons are a primary target of the *tippy* mutation. Furthermore, we hypothesize that the

*Correspondence: Kathleen J. Millen, PhD, Seattle Children's Research Institute, Center for Integrative Brain Research and 1900 Ninth Avenue Mailstop JMB-10, Seattle WA 98101, 206-884-3225 office, 206-884-1210 fax, kathleen.millen@seattlechildrens.org.

Conflict of interest notification

All authors have nothing to disclose.

Purkinje cell axonal pathology together with disruptions in the balance of climbing fiber and parallel fiber Purkinje cell input in the cerebellar cortex underlie the ataxic phenotype in these mice. The constellation of Purkinje cell dendritic malformation and degeneration phenotypes in *tippy* mutants is unique and has not been reported in any other neurologic mutant. Fine mapping of the *tippy* mutation to a 2.1MB region of distal chromosome 9, which does not encompass any gene previously implicated in cerebellar development or neuronal degeneration, confirms that the *tippy* mutation identifies novel biology and gene function.

Keywords

cerebellum; climbing fibers; dendritogenesis; Purkinje cell degeneration; spinogenesis

Introduction

Many classical spontaneous neurological mutants exhibit cerebellar dysfunction or ataxia (Sidman et al., 1965). These mutant mice have provided fundamental knowledge regarding the pathways critical for the development and function of the cerebellum which have also translated to other CNS regions and have advanced our understanding of the pathogenesis of human neurological disease (Grüsser-Cornehls and Bäurle, 2001; Hirano, 2006; Meisler et al., 1997). The Jackson Laboratory Mouse Genome Informatics database (www.informatics.jax.org) currently lists 446 spontaneous neurological mutant alleles, many of which have been annotated with molecular mechanism. However, numerous mutants still exist whose genetic lesions and detailed cellular and molecular phenotypes remain uncharacterized, representing a rich, yet untapped, resource for defining gene function and novel underlying biology.

The *tippy* mouse represents one such understudied mutant. The *tippy* mutation arose during a linkage cross at Jackson Laboratory in 1977. Homozygous *tippy* mutant mice are small, severely ataxic, and typically die by postnatal day 20 (P20). Although the *tippy* behavioral phenotype suggests cerebellar and/or vestibular abnormalities, previous studies found no anatomical alterations explaining the neurological symptoms (Lane and Bronson, 1995). The *tippy* mutation was initially mapped to distal chromosome 9 and is non-allelic to the nearby *ducky* (*Cacna2d*), another spontaneous mutant locus associated with ataxia (Barclay et al 2001). While several candidate genes have been proposed in past years, including the molecular lesion remains unknown.

Through detailed anatomical and electrophysiological studies of *tippy* homozygous mutants, we have uncovered a complex cerebellar phenotype that primarily involves Purkinje cells in both their somatodendritic and axonal compartments. We observed widespread alterations of the Purkinje cell dendritic arbor, anomalous parallel fiber-Purkinje cell electrophysiology, dystrophy of the cell organelles including mitochondrial clumping, endoplasmic reticulum vesiculation, axonal torpedo and severe changes of Purkinje axon terminals in the cerebellar cortex, as well as in the cerebellar nuclei and the vestibular nuclei. These changes were accompanied by patchy, caspase-3 independent, dark degeneration of the Purkinje neurons and widespread microglial and astroglial activation throughout the cerebellar cortex and its

target nuclei. The data suggest that the Purkinje cells are a major target of the *tippy* mutation, which our genetic analyses indicate to be a heretofore unrecognized player in cerebellar development and degeneration. This constellation of developmental and degenerative phenotypes is unique and to the best of our knowledge has not been described in any other neurological mutant. Further analysis of this mutant will therefore provide fundamental novel insights into Purkinje cell biology, which in turn, is likely to provide invaluable information regarding the cause of human cerebellar ataxias of unknown etiology.

Materials and Methods

Animals and Chemicals

Heterozygous *tippy* mice (Jackson Laboratory stock #001055; maintained on C57BL/6;C3HeB/Fe genetic background) were originally obtained from the Jackson Laboratory and interbred in-house. Homozygous mutant mice were distinguished from their heterozygous *tippy* and homozygous control littermates by ataxic gait and small body size. Analysis was conducted with interbred mice from generations 1–5. No evidence was seen of the phenotype changing across generations. A few homozygous *tippy* mice were nursed beyond P20. Unaffected littermates and wild-type mice were used in the experiments as controls. Control C3HeB/Fe (stock #000658) and Molf/E_i (stock #000550) strains were also purchased from Jackson Laboratory. Mice between the ages of P10–P35 were deeply anesthetized with i.p. sodium pentobarbital (60mg/kg body weight) and transcardially perfused with appropriate fixatives. This study was carried out on mice in strict accordance with the recommendations in the Guide for the Care and Use of Laboratory Animals of the National Institutes of Health. All chemicals were purchased from Sigma-Aldrich unless otherwise stated.

Tissue Processing, Histology, and Immunohistochemistry

Mice between the ages of P10–P35 were transcardially perfused with 4% freshly depolymerized paraformaldehyde (PFA) in phosphate buffered saline (PBS). Dissected brains were postfixed for 2 to 48 hours at 4°C and washed with PBS followed by various tissue processing protocols. Paraffin sections (12 μm-thick) were generated and processed for immunocytochemistry according to avidin/biotin amplification protocol using diaminobenzidine (DAB) as chromogen. Agarose-embedded 50 μm-thick tissue sections cut on a vibrating blade microtome, 20 μm-thick cryosections cut on a cryostat or 24 μm-thick frozen sections cut on a freezing stage microtome were processed for immunohistochemistry as reported (Hirai et al., 2005; Chizhikov and Millen, 2004; Sekerková et al., 2007). Sections were labeled with the following primary antibodies: rabbit anti-calbindin D28k (1:2000, Swant), rabbit anti-GABAα6 receptor (1:100, Millipore), rabbit anti-glial fibrillary acidic protein (GFAP) (1:500, DAKO), rabbit anti-parvalbumin (1:200, Swant), guinea pig anti-vesicular glutamate transporter 1 (VGluT1) (1:500-5,000; Millipore), guinea pig anti-VGluT2 (1:500-5,000, Millipore), rabbit anti-PEP19 (1:3,000; generous gift of Dr. J.I. Morgan, St. Jude, Memphis, TN), rabbit anti-cleaved capase-3 (Casp3) (1:50, Cell Signaling), rabbit anti-calretinin (1:5,000, Swant), and mouse anti-ubiquitin (1:3,000, Fitzgerald Industries International). Secondary antibodies were from goat or donkey and were conjugated to biotin (1:200, Jackson ImmunoResearch; 1:500, Amersham), to Alexa

Fluor-488 or 568 (1:100, Invitrogen), or Dylight 488 or 594 (1:400, Jackson ImmunoResearch). Gelatin embedded 20 μm-thick sections were used for Nissl staining (Chizhikov et al., 2007). Slides bearing frozen cut tissue were stained with Fluoro-Jade C (Millipore) (Schmued et al., 2005). Terminal deoxynucleotidyltransferase-mediated dUTP nick end labeling (TUNEL) assay was performed using In Situ Cell Death detection kit, (POD, Roche Diagnostics). For Golgi staining, dissected brains of P21 mice were processed using the FD Rapid GolgiStain™ Kit (FD NeuroTechnologies). After Golgi-Cox impregnation, 100 μm cryosections were counterstained as outlined in the GolgiStain™ Kit.

Electron Microscopy

For electron microscopy, mice were perfused with saline followed by a fixative containing 2% freshly depolymerized PFA and 1% purified glutaraldehyde (Electron Microscopic Sciences) in 0.12M phosphate buffer (PB). Cerebella were removed, postfixed for 24 h at 4°C and sliced on vibrating blade microtome at 100 μm in the coronal or sagittal plane. Slices were postfixed in buffered 2% OsO_4, rinsed, stained in 1% uranyl acetate, dehydrated, and embedded in Epon. Semithin sections, 1–2 μm thick, were cut on an ultramicrotome, collected on gelatin-coated slides and stained with toluidine blue. Ultrathin sections were contrasted with lead citrate and uranyl acetate, and analyzed under a Zeiss EM-10 electron microscope operated at 60–80 kV.

Anterograde Labeling

Control ($n = 6$) and *tippy* mutant ($n = 6$) P21 mice were transcardially perfused with 4% PFA. Dissected brains were postfixed for 2 hours at 4°C and washed with PBS. Four to six medium-sized cohesive DiI crystals (Molecular Probes, Invitrogen) were picked up with the tip of a fine Tungsten needle and inserted, under a dissecting microscope, into the right and left inferior olivary nuclei. The brains were subsequently stored in PBS with 0.2% sodium azide at 37°C for 2 weeks followed by storage at room temperature for 9 months in the dark to allow for diffusion of the DiI (Faust, 2003). Free-floating 50 μm agarose-embedded sections were processed for immunostaining as previously described (Matsubayashi et al., 2008).

Slice Preparation and Electrophysiological Recording

After isoflurane anesthesia and decapitation, parasagittal slices of cerebellar vermis (250 μm thick) were prepared from P20–P24 mice in ice-cold artificial cerebrospinal fluid (ACSF) containing (in mM): 124 NaCl, 5 KCl, 1.25 Na_2HPO_4, 2 $MgSO_4$, 2 $CaCl_2$, 26 $NaHCO_3$ and 10 D-glucose bubbled with 95% O_2 and 5% CO_2. For recording, slices were continuously perfused with ACSF supplemented with 100 μM picrotoxin to block $GABA_A$ receptors at 31–34°C. Whole-cell voltage-clamp recordings were performed from visually identified Purkinje cells with a patch pipette that had a resistance of 2–3 MΩ when filled with an internal solution consisting of (in mM): 150 CsCl, 0.5 EGTA, 10 HEPES, 8 sucrose, 4 Na-ATP and 0.4 Na-GTP adjusted to pH 7.3 with CsOH. Ionic currents were recorded with an EPC-10 amplifier (HEKA Elektronik, Lambrecht/Pfalz, Germany). Signals were filtered at 1.5 or 2.9 kHz and digitized at 10 kHz and the liquid junction potential was compensated unless otherwise stated.

Parallel fiber (PF) and climbing fiber (CF) responses were induced by electrical stimulation (200 μs pulse) to the molecular layer and granular layer of the cerebellum, respectively. For extracellular stimulation, the standard pipettes filled with external ACSF were used. CF-EPSCs were recorded with membrane potentials held at −70 mV and −20 mV. CF-EPSCs were identified by their all-or-none response and paired-pulse depression (PPD). PF-EPSCs were recorded at −70 mV, and they were identified by their graded development to smoothly increasing stimulus intensity and paired-pulse facilitation (PPF). To search for multiple CF innervation, the intensity of stimulation was gradually increased from 0 to 70 μA by 5 μA increments and the number of amplitude steps in evoked EPSCs was counted. EPSCs were recorded from Purkinje cells, irrespective of dendritic morphology. For evoked-EPSC recording, 5-mM QX-314 (Tocris Cookson) was included in the internal solution to avoid action potential generation. Miniature excitatory postsynaptic currents (mEPSCs) were recorded from Purkinje cells at a holding potential of −80 mV, under the bath-application of 1 μM tetrodotoxin (Tocris Cookson, Bristol, UK,). The mean amplitude was calculated from more than 150 mEPSC events for each recording.

Image Acquisition, Analysis and Quantification

Sections were analyzed with a Zeiss Axiovert 2100TV inverted microscope or Nikon Eclipse E800 microscope. Bright field and immunofluorescence images were acquired with a Spot RT CCD video camera (Diagnostics Instruments). Laser scanning confocal analysis was performed with a Leica SP2 AOBS spectral confocal microscope or Nikon PCM 2000 Confocal Microscope System. Projections of confocal z-stacks were acquired using ImageJ (10–50 slice Z-series separated by 0.5 μm). Images were processed with ImageJ in conjunction with Adobe Photoshop (Adobe Systems Inc.). Electron micrographic negatives were scanned and imported into Adobe Photoshop CS for image processing. Confocal stack projections of parasagittal cerebellar sections co-labeled for calbindin and VGluT2 from control (n = 10 images from 4 mice) and *tippy* mutant mice (n = 11 images from 4 mice) were used for analysis of CF innervation territory. Molecular layer thickness was measured from the base of the Purkinje cell somas to the pial border. CF-terminal reach was measured from the base of the Purkinje cell somas to the most distal tip of continuous VGluT2-positive terminals. The CF innervation territory was determined by taking the ratio of CF-terminal reach/molecular layer thickness. Student's t-test was used unless otherwise stated.

Genetic Mapping

Tippy mice were maintained on C57BL/6;C3HeB/Fe and outcrossed to both male and female Molf/E_i for mapping. Affected F_2 progeny (n=226) of F_1 intercrosses were identified based on ataxic gait at P14–P18. Initial genotyping was performed using a single nucleotide polymorphism (SNP) panel of 768 autosomal markers (Moran et al., 2006; Ideraabdullah et al., 2007). Linkage analysis was performed across each autosome using Allegro 2.0 (Gudbjartsson et al., 2005). Parametric LOD scores were calculated assuming a fully penetrant recessive mode of inheritance and a disease allele frequency of 1/10,000. Fine mapping was with informative MIT microsattelite markers and published SNPs on chromosome 9 using standard PCR protocols (available upon request). Amplification products were electrophoresed on 5–10% polyacrylamide gels. An enzymatic cocktail containing exonuclease I (10 U/μl; USB) and shrimp alkaline phosphatase (1 U/ μl; USB)

was used to degrade primers and dNTP prior to sequencing. Sequences from both strands were obtained using an ABI 3730XL 96-capillary Genetic Analyzer (Applied Biosystems) at the University of Chicago Cancer Research Center DNA Sequencing Facility and analyzed using Mutation Surveyor software.

Results

Purkinje cell dendritic branching and spine abnormalities in homozygous tippy mutant mice

Homozygous *tippy* mutant mice were distinguishable from their littermates (heterozygous *tippy* and control C57BL/6;C3HeB/Fe) by age P10 based on reduced body size and failure to acquire a normal righting reflex. Confirming previous reports (Lane and Bronson, 1995), mutant cerebellar morphology was grossly normal with no observable defects in the structure of the vermis or cerebellar hemispheres (Fig. 1*A,B*). Nissl stained mid-sagittal cerebellar sections revealed no marked differences in foliation or tri-laminar organization between control and mutant mice (Fig. 1*C,D*). The cerebellum, however, was disproportionately small relative to overall brain size in homozygous mutant mice.

A careful examination of the various cell populations constituting the cerebellar cortex at both P35 and P21 revealed specific defects in mutant Purkinje cells. In Golgi impregnated sections or after calbindin or PEP19 immunostaining, Purkinje cells from control mice exhibit a highly stereotypic dendritic branching pattern of 1–2 1st order branches emerging from the cell soma followed by 2nd order and tertiary branches, with spiny branchlets coming off only at the tertiary level or above (Fig. 1*E*). In contrast, homozygous *tippy* mutant Purkinje cells often possessed no clear secondary or tertiary dendritic branches and distal spiny branchlets emerged directly and abundantly from the primary dendritic stem, even in its proximal region (Fig. 1*F*, arrowheads). Approximately 25% of *tippy* mutant Purkinje cells retained the control dendritic architecture and of those that displayed a branching defect, there was a range in the severity of the malformation, with some mutant cells displaying the proximal overbranching of spiny branchlets while possessing clear secondary dendritic shafts. Abnormal Purkinje cells were observed in all lobules, across the vermis and both hemispheres and we found no evidence to suggest that they were restricted to sagittal domains. Differences in branching morphology were evident as early as P10 (data not shown). Analysis at earlier ages was precluded by the ability to identify mutant mice based solely on ataxia.

We next performed Golgi staining studies on cerebella of control (Fig. 1*G*) and mutant mice (Fig. 1*H*) at P21 to view individual Purkinje cells in isolation. These studies confirmed the branching defect and revealed additional mutant Purkinje cell phenotypes. First, homozygous *tippy* mutant Purkinje cells exhibited meandering arbors with an apparent loss of the characteristic strict planarity of Purkinje cells. Homozygous mutant Purkinje cell processes were also more clustered and appeared overlapping in their coverage, unlike the control Purkinje cell dendritic branches and spines, which spread out evenly over an area, suggesting defects in dendritic self-avoidance. Third, in contrast to the control Purkinje cells, which possessed dendritic spines of a mature morphology with a distinct head and neck, mutant Purkinje cells often displayed thin, elongated filopodia characteristic of

immature neurons, indicating a dendritic spine malformation. Moreover, in the mutant, many more spines than normal were located along the proximal dendritic shaft as well as the cell soma (Fig. 1*H*, *insets*), yielding a cellular architecture reminiscent of immature Purkinje cells with multiple perisomatic processes as well as Purkinje cells deprived of afferent input. These spine abnormalities were visible even on homozygous *tippy* mutant Purkinje cells with normal dendritic arbors.

To determine if other cerebellar cell types had abnormal morphology or distribution, we performed immunohistochemical studies with a series of cell-type specific markers. We observed that granule cells formed a compact layer of normal density, and stellate and basket cells were confined to their correct positions with no marked difference in density in homozygous *tippy* mutant mice. Golgi, Lugaro and unipolar brush cells were properly positioned with normal morphology, although their numerical densities were not analyzed. Bergmann glial cells also displayed no positional or organizational defects. We did, however, observe marked upregulation of GFAP in both Bergmann glia and astroglial cells of the granular layer, white matter and deep nuclei (data not shown), suggesting widespread glial activation.

Purkinje cell dystrophy and degeneration in the homozygous tippy mutant cerebellum

Immunohistochemistry with the Purkinje cell-specific marker, PEP19 (Fig. 2*A–F*) (Mugnaini et al., 1987) confirmed the dendritic branching abnormalities originally observed with calbindin and also revealed additional abnormalities in homozygous *tippy* mutants. Co-labeling with PEP19 and ubiquitin identified multiple ubiquitin-positive and PEP19-negative Purkinje cells distributed throughout the Purkinje cell layer in P18 homozygous *tippy* mutants, interspersed with ubiquitin-negative Purkinje cells (Fig. 2*B*), some of which showed dystrophic signs by PEP19 staining alone (Fig. 2*C*). No ubiquitin-positive cells were found in control mice (Fig. 2*A*). PEP19 immunolabeling also identified axonal swellings, or torpedos at the level of the initial Purkinje cell axon segment and within the core of the cerebellar folia white matter of *tippy* mutant mice (Fig. 2*D–F*). Staining for Fluoro-Jade C, a fluorescent high-resolution selective dye for neurodegeneration (Schmued et al., 2005), was present in dendrites, soma (Fig. 2*H*) and axons (Fig. 2*I*) of *tippy* mutant Purkinje cells, but was absent in controls (Fig. 2*G*). This confirmed that all compartments of the Purkinje neuron were degenerating, as further demonstrated in semithin and electron microscopic sections (Figs. 2*J–M*, 3, 4). Notably, the majority of degenerating Purkinje cells were concentrated in the anterior lobe (lobules I–V) and in the banks of the secondary fissure (Lobules VIII and IX). On average, we observed 20–40 degenerating Purkinje cells per sagittal vermal section. Notably, the degenerating Purkinje cells did not conform with typical parasagittal stripes seen in other mutants (Sarna and Hawkes 2003). Further studies will be needed to address if the degeneration of Purkinje cells follows a particular pattern or it is a random process.

We next searched for signs of degenerations in the deep regions targeted by the Purkinje cell axons. Large numbers of enlarged, PEP-19 positive axonal processes and perisomatic terminals were present throughout the vestibular and cerebellar nuclei of *tippy* mutant mice (Fig. 3*A,B*) in contrast to controls (Fig. 3*C*). Conspicuously, the number of dysmorphic

axonal profiles in the cerebellar and vestibular nuclei observed in PEP19 stained semithin sections by far exceeded that of the Fluoro-Jade C positive profiles observed in the same locations (Fig. 3*D*), suggesting that the number of dystrophic processes outnumbered those undergoing advanced degeneration.

Semithin sections of homozygous *tippy* mutants treated with toluidine blue revealed neurons in intermediate (delicately stained) and advanced stages (dark stained) of degeneration, with degenerating dendrites in the molecular layer showing abnormal contrast, which was never observed in control mice (Fig. 2*J–M*, inset in Fig. 4*C*). Most of the dark-staining cells were intermingled with negative cells, but we also observed multiple affected cells in sequence in rare instances (Fig. 2*K*). Occasionally, degenerating cells in one folium appeared in register with degenerating cells in a neighboring folium. TUNEL labeling and immunostaining for activated caspase3 failed to detect any staining in either *tippy* mutants or control cerebella (data not shown). Notably, in all of our studies of Purkinje cells in *tippy* mutants from P16–21, we did not find evidence of extensive “holes” in the Purkinje cell monolayer suggesting that the Purkinje cell loss is a slow process. Further, Fluoro-Jade C staining of sections from elsewhere in the brain revealed that degenerative processes were restricted to cerebellar Purkinje cells; in particular, no degeneration was present in the inferior olivary complex (data not shown)..

Electron microscopic analysis confirmed the presence of subtle alterations as well as conspicuous abnormalities (Figs. 4 and 5) in individual and small groups of Purkinje cell bodies and dendrites indicative of both early and advanced degenerative processes in homozygous *tippy* mutants that were not observed in control littermates. Purkinje cells in P18 control mice commonly possessed qualitatively normal structural features (Figs. 2*J*, 3*F*, 5*A*). The perikarya and proximal dendrites of the unaffected Purkinje cells in *tippy* mutants were usually surrounded by the cell bodies and slender processes of Bergmann glia; the basket cell axons formed synapses on the smooth portions of the somatic and dendritic plasma membrane, while the climbing fibers CFs formed synapses mainly on the spines emanating from the proximal trunks; stellate cell axons contacted the stems of the distal dendrites and PFs contacted the spines of the spiny branchlets (see Larramendi and Victor, 1967; Palay and Chan-Palay, 1974; Sotelo,1990).

Notably, abnormalities in mutant cerebella encompassed cell somata (Fig. 4*B,C*), the entire dendritic arbor in the molecular layer including the dendritic spiny branchlets (Fig. 5), initial axon segments and white matter fibers (Fig. 4*D–F*) as well as the Purkinje cell axon terminals in the cerebellar nuclei and lateral vestibular nuclei (Fig. 3).

Early signs of alteration in the Purkinje cell bodies consisted mainly of an increase of the electron density of the cytoplasm and dilatation of the cisterns of the Golgi apparatus and the endoplasmic reticulum, and an increase in the number of multivesicular endosomes, lysosomes, double-membrane bound authophagosome-like and autolysosome-like bodies (Fig. 4B). Clumping of the mitochondria, however, was observed only occasionally. Purkinje cell bodies in advanced stages of degeneration appeared shrunken, with marked density of the cytoplasm and the nuclear content and were surrounded by swollen profiles of the

Bergmann glia and by microglial phagocytes; the perikaryon contained prominent vacuoles, dilated cisterns of the endoplasmic reticulum and clumped organelles (Fig. 4C).

Ultrastructural cytoplasmic alterations in the mutant Purkinje cell dendritic arbors consisted of dilation of individual cisterns of the endoplasmic reticulum (Fig. 5*A*), an abnormally high frequency of cytoplasmic vesicles (Fig. 5*D,H*), the occurrence of numerous multivesicular endosomes, lysosomes, double-membrane bound authophagosome- and autolysosome-like bodies (Fig. 5*D,H*), the formation of loose mitochondrial aggregates (Fig. 5*A,E,F,G*) and an increase in the electron opacity of the cytoplasm (Fig. 5*A–H*). In the spiny branchlets, these changes were frequently accompanied by long, slender spines with extremely narrow necks (Fig. 5*B,F*). More severe dendritic changes were mainly characterized by the conspicuous beading of the large dendritic stems and shrinkage of the spiny branchlets, the formation of large masses of dilated and vesiculated endoplasmic reticulum and clumps of enlarged or fused mitochondria in the center of the dendritic trunks accompanied by a marked electron density of the cytoplasm that obfuscated the profiles of microtubules and neurofilaments, most of which were situated in a peripheral ring beneath the plasma membrane (Fig. 5*F–H*). Notably, synaptic junctions of PFs (Fig. 5*B*) and CFs (Fig. 5*C*) were still recognizable in many of the degenerating dendrites. The degenerating arbors were surrounded by dilated profiles of Bergmann glia (Fig. 5*C,E–G*) and by the processes of microglial cells (Fig. 5*G,H*), some of which were traced to parent cell bodies situated along the blood vessels (data not shown). Some of the degenerating dendrites were engulfed by microglia profiles together with their surrounding Bergman glial processes (data not shown)

Numerous Purkinje cell axons in the folial white matter and in the cerebellar and vestibular nuclei presented distinct torpedoes and spheroids, containing autophagosome-like and autolysosome-like bodies and swollen endoplasmic reticulum, as well as dark axoplasmic degeneration (Fig. 3*D,E*). These alterations were accompanied by prominent dystrophic changes in the Purkinje axon terminals in all the sites in which they are known to occur (i.e., upper granular layer, lower molecular layer, cerebellar nuclei and vestibular nuclei; Palay and Chan-Palay, 1974). The dystrophic terminals contained enlarged mitochondria, lysosomes, dilated cisterns of the smooth endoplasmic reticulum and clustered synaptic vesicles immersed in a granulo-fibrillar cytoplasm of medium electron density (Figs. 3*E*).

In contrast, no overt alterations were observed in the targeting of the CFs and parallel fibers (PFs), and the axons of the basket and stellate cells in the unaffected and degenerating homozygous *tippy* Purkinje cells, although CF synapses on cell body spines and smooth dendritic trunks occurred more frequently than in the Purkinje cells of control littermates (data not shown). Notably, we found minimal evidence that other types of cerebellar neurons were directly affected in *tippy* mutants (data not shown).

Altered climbing fiber-Purkinje cell innervation in homozygous tippy mutants

Although Purkinje cell pathology appeared to be an important feature of the *tippy* phenotype, only a subset of mutant Purkinje cells showed obvious signs of neurodegeneration. Some features of the non-degenerative mutant Purkinje cells have been observed in other cerebellar mutants. For example, hyperspiny shaft dendrites and soma have been previously described in Purkinje cells deprived of CF innervation (Sotelo, 1975a,

1975b, 1976, Rossi et al., 1991, Cesa et al., 2003). We therefore examined CFs in more detail. Nissl stained sections illustrated that the inferior olivary nuclei, the sole source of climbing fibers, were grossly normal in mutant mice at P21 (Fig. 6*A*). To assess the distribution of CF terminals within the molecular layer, we co-labeled Purkinje cells for calbindin and vesicular glutamate transporter 2 (VGluT2), which is specifically expressed in CF terminals in the cerebellar cortex at P21 (Ichikawa et al., 2002). As in control cerebella, there was a clearly demarcated proximal domain of VGluT2-immunopositive puncta in the molecular layer of homozygous *tippy* mutant cerebella (Fig. 6*C,G*), with no distal expansion of the CF territory, which has been observed with loss of PF-Purkinje cell synaptic connections (Hirai et al., 2005). However, there was a proximal retraction of the normal CF domain in mutant mice compared to control mice, with CF terminals encompassing 83.3 ± 1.6% of the molecular layer thickness in control mice versus 68.9 ± 1.5% in mutant mice ($p < 0.00001$; Fig. 6*E*). Of note, there was no significant difference in the molecular layer thickness between control and mutant mice (data not shown). Furthermore, CF terminals were associated with only shaft dendrites in both control and mutant mice and there were no shafts observed that were free of VGluT2-positive puncta, suggesting the decreased CF domain was a consequence of an underlying reduction of synaptically adequate shaft area on mutant Purkinje cell arbors rather than available CF territory that remained uninnervated.

Although the overall density of VGluT2-immunopositive puncta within the molecular layer did not appear markedly different (Fig. 6*C,G*), the density of VGluT2 terminals on individual Purkinje cells appeared higher in mutant cerebella compared to controls (Fig. 6*D,H*). This increased density was most apparent as a marked clustering of VGluT2-positive puncta in *tippy* mutant mice, most prominently in the proximal portions of the dendritic tree (Fig. 6*H*). This stood in stark contrast to the control cerebella, in which the VGluT2-positive puncta, all of similar size, were regularly spaced along the Purkinje cell dendritic branches (Fig. 6*D*). Furthermore, VGluT2-labeled CF terminals were present on the cell bodies of *tippy* mutant Purkinje cells that were never seen in control cerebella.

To examine the pattern of CF innervation at single-fiber resolution, we performed a triple labeling anatomical study utilizing anterograde DiI tracer labeling from the inferior olivary nuclei, anti-VGluT2 to visualize all CF terminals and anti-calbindin to visualize Purkinje cell dendrites. In the control mice, each CF demonstrated a clear 1:1 relationship with individual Purkinje cells with single DiI-labeled CFs traversing the cerebellar white matter via a direct route, ascending through the Purkinje cell layer past the cell bodies and winding around the proximal dendritic shaft, branching regularly, up to the point of intersection of shaft dendrites with spiny branchlets (Fig. 6*I,J*). In contrast, the *tippy* mutant DiI-labeled CFs often twisted through the Purkinje cell layer, intermingled with other DiI-labeled fibers (Fig. 6*K*, arrowheads), and wrapped extensively around the cell body of Purkinje cells prior to encircling the dendritic shafts (Fig. 6*L*). Colocalization of VGluT2 puncta and DiI-labeled fibers indicated aberrant synaptic contacts between the CFs and mutant Purkinje cells on the cell bodies (Fig. 6*L*). We also observed an increased thickness of the DiI-labeled CFs on mutant Purkinje cells, suggesting decreased branching and possibly increased number of wrap-arounds of the dendritic tree by each CF. Concurrently, there appeared to be a higher number of DiI and VGluT2 co-labeled puncta on the mutant Purkinje cells, most notably on the proximal dendritic shaft. Lastly, while all VGlut2-positive terminals on individual

Purkinje cells were associated with a DiI-labeled CF in control cerebella (Fig. 6*J*), a small minority of mutant Purkinje cells possessed DiI-labeled CF/VGluT2-positive puncta on the same dendrites as tracer-unlabeled/VGluT2-labeled terminals, indicating innervation by multiple CFs (Fig. 6*L*, arrowhead).

Unaltered EPSC amplitude of Purkinje cell-climbing fiber synapse in homozygous tippy mutant mice

To determine the functional relevance of the anatomical alterations, we undertook an electrophysiological analysis to evaluate synaptic interactions in the cerebellar cortex of control and homozygous *tippy* mutant mice. We first examined excitatory postsynaptic currents (EPSCs) in response to CF (or PF) stimulation in P21–P24 slice preparations by whole-cell patchclamping (Fig. 7*A*). CF-evoked EPSCs were identified by their characteristic all-or-none nature and by the presence of paired-pulse depression (PPD) following two stimuli delivered within a short time window (Llinás and Sugimori, 1980; Crepel et al., 1981; Konnerth et al., 1990; Perkel et al., 1990). After the recruitment of the first CF, multiple innervation was detected by a stepwise increase of the EPSC following a graded increase in the stimulus intensity. Most Purkinje cells in both control (n = 22 cells) and homozygous *tippy* mutant (n = 15 cells) mice exhibited single-step CF-EPSCs, indicating monoinnervation (Fig. 7*B*). However, in some Purkinje cells a second discrete current step appeared as the stimulus intensity was increased, indicating multiple innervation, consistent with the tracer-labeling data; the differences, however, were not statistically significant ($p > 0.6$, Mann-Whitney test). Therefore, the elimination of supernumerary CFs from Purkinje cells during development is not fundamentally impaired in *tippy* mutant mice.

To determine the synaptic strength of CFs on Purkinje cells in control and mutant mice, we recorded the maximum amplitude of CF-EPSCs from Purkinje cells at a holding potential of either −70 mV or −20 mV. Surprisingly, there were no significant differences in the amplitudes of CF-EPSCs between control (n = 7 cells) and mutant (n = 6 cells) mice at both holding potentials (Fig. 7*C*), indicating that despite the alterations in the distribution, density, and size of CF terminals in homozygous *tippy* mutants, the strength of the net response evoked in the mutant Purkinje cells is the same as in control mice. In addition, CF-EPSCs in mutant cerebella (n = 9 cells) exhibited PPD over a range of inter-stimulus intervals that was not significantly different from control mice (n = 9 cells; Fig. 7*D*), indicating that this measure of short-term plasticity at Purkinje cell-CF synapses is normal in homozygous *tippy* mutant mice.

Decreased EPSC amplitude of Purkinje cell-parallel fiber synapse may reflect decreased parallel fiber-Purkinje cell synaptic contacts in homozygous tippy mutant mice

We next measured EPSCs from Purkinje cells in response to PF stimulation, which reflect input from granule cells. As with the CF-evoked EPSCs, PF-EPSCs exhibited normal short-term plasticity in both control (n = 17 cells) and *tippy* mutant (n = 14 cells) mice, demonstrating paired-pulse facilitation (PPF) at interpulse intervals between 10 and 500 ms (Fig. 7*D*). However, the maximum amplitudes of PF-EPSCs in homozygous *tippy* mutant Purkinje cells (n = 19 cells) were consistently smaller than those in control Purkinje cells (n

= 13 cells) over a broad range of stimulus intensities (10–70 μA; Fig. 7*E*), indicating impaired PF-Purkinje cell synaptogenesis. Importantly, as PPF reflects presynaptic functions and this measure was normal in *tippy* mutant mice, the decreased PF-EPSC amplitudes indicate probable defects on the postsynaptic side in mutant Purkinje cells or alterations in the number of functional contacts between PFs and mutant Purkinje cells.

To determine if the decreased PF-EPSC amplitude in homozygous *tippy* mutant mice was associated with changes at individual synapses, we recorded spontaneous excitatory activity in the cerebella of *tippy* mutant mice and their littermates. Miniature excitatory postsynaptic currents (mEPSCs) were recorded from parasagittal cerebellar slices under the bath application of tetrodotoxin (TTX) (Fig. 7*F*). The average frequency of mEPSCs in control mice was 1.92 ± 0.18 Hz ($n = 17$), which was not significantly different from the frequency measured in *tippy* mutant mice (2.07 ± 0.26 Hz, $n = 21$; Fig. 7*G*). Therefore, the number of synaptic connections on mutant Purkinje cells is likely unaltered. In contrast, the amplitude of mEPSCs was significantly decreased in mutant mice (6.04 ± 0.17 pA) compared to control mice (7.92 ± 0.32 pA; $p < 0.0001$; Fig. 7*H*), suggesting a change in presynaptic quantal content or postsynaptic changes in receptor density or composition in homozygous *tippy* mutant cerebella. Of note, the recorded mEPSCs could not be localized specifically to either CF- or PF-Purkinje cell synapses but represented spontaneous activity at both excitatory synapses.

The decreased PF-EPSCs in homozygous *tippy* mutant mice suggested a potential loss of mossy fiber contact with granule cells or PF contact with Purkinje cells. At a gross level, Nissl stained sagittal sections demonstrated structurally intact pontine nuclei—a major source of mossy fibers—in both control and mutant mice (Fig. 8*A,F*). A loss of PF synaptic contacts with Purkinje cells in mutant cerebella is consistent with the fragmented and degenerating Purkinje cell dendrites observed in homozygous *tippy* mutants (Figs. 2, 3), although EM analysis suggests that up to substantially advanced stages, degenerating Purkinje cells maintain synaptic contact with both CF and PFs (Fig. 3*A,B*). To more globally assess the pattern of PF innervation of Purkinje cells in control and mutant mice, we labeled PF terminals with antibodies to vesicular glutamate transporter 1 (VGluT1) and Purkinje cells with calbindin. No discernable differences in the distribution or overall density of VGluT1-immunopositive puncta were observed between control and mutant mice (Fig. 8*C,H*), indicating no marked loss of PF terminals in the mutant cerebellum. However, while there was a homogeneous overlay of calbindin-immunopositive Purkinje cell processes and VGluT1- positive PF terminals in control mice (Fig. 8*D,E*), there were regions of VGluT1-positive staining without corresponding calbindin-labeled Purkinje cell dendritic partners in homozygous *tippy* mutant mice (Fig. 8*I,J*, boxed regions), suggesting presynaptic terminals without postsynaptic partners in patchy regions throughout the cerebellar cortex with no discernable pattern.

The tippy genetic lesion represents new molecular control of Purkinje cell biology

The homozygous *tippy* mutant Purkinje cell morphological and electrophysiological phenotypes are unique, suggesting that the underlying mutation is likely to be a novel regulator of Purkinje cell dendrite development and neuronal survival. We therefore

established an intersubspecific intercross with *Mus mus molissinus* (Molf/E_i) to map the mutation (Fig. 9*A*). Linkage analysis of data from 8 ataxic F2 mice on a 768 SNP panel (Ideraabdullah et al., 2007) revealed maximum evidence for linkage of the *tippy* mutation (LOD = 3.3) within a 26 cM (37.0 Mb) region between SNP markers rs3698443 and rs8254399 (data not shown). Subsequent fine mapping using DNA from 208 ataxic P14–P18 F2 offspring mapped the *tippy* locus to a 1.0 cM (2.1 Mb) interval on distal chromosome 9, between markers rs33627650 and rs3714504 (Fig. 9*B*). Haplotype results revealed that the *tippy* mutation originally arose on a C3H/Fe chromosome and three markers (rs30330775, D9MIT24, rs29937959) remained completely linked with the *tippy* phenotype (Fig. 9*C*). This 2.1 Mb critical region (chr9:101789046-103916280, UCSC Genome Browser Build 37) contains ~23 genes (Supplementary Table 1). None of these genes have been previously implicated in cerebellar development or neuronal degeneration.

Discussion

Our data implicate Purkinje cells as the major target of the *tippy* mutation, with other neuronal cell populations in the cerebellum remaining grossly normal. The mutant Purkinje cell phenotype is a combination of abnormal dendritogenesis and degeneration. To our knowledge, this combination is unique amongst all cerebellar mouse mutants described to date. The mutation maps within a 2.1 Mb critical region of chromosome 9 encompassing 14 characterized genes and 6 ESTs, none of which have been previously implicated in cerebellar development or neuronal degeneration.

We have focused our analysis on postnatal cerebellar development in the *tippy* mutant, since without specific knowledge of the underlying molecular lesion, we are limited to identifying the mutants based on their smaller body size and ataxia, which cannot be definitively assessed earlier than P10–12. The disproportionately small size of the postnatal homozygous *tippy* mutant cerebellum may in large part reflect abnormalities of the somatodendritic and axonal compartments of the mutant Purkinje cells. Nevertheless, we cannot rule out earlier abnormalities in Purkinje cell and granule cell neurogenesis that could also contribute to the reduced size.

Tippy mutants exhibit a unique constellation of Purkinje cell dendritic phenotypes

Although individual aspects of the *tippy* dendrite and spine phenotypes are shared by other murine mutants, *tippy* presents several challenges to current paradigms of dendritogenesis and spinogenesis (Kapfhammer, 2004). For example, Purkinje cell dendritic trees in *tippy* mutants exhibit loss of sagittal planarity—a reported consequence of PF input loss in mutants. However, we see preserved PF input in *tippy* mutants. Further, higher-order distal spiny branchlets, the principal category of dendritic processes absent in PF-deprived Purkinje cells, such as in *weaver* mutants (Rakic and Sidman, 1973), are also preserved in *tippy* mutants.

Since spine shape and formation are significantly affected by synaptic activity (Hering and Sheng, 2001), it remains possible that the defects demonstrated by homozygous *tippy* mutant Purkinje cell dendritic spines are a consequence of alterations in physiological activity. Indeed, there is such a “hyperspiny transformation” in response to CF deprivation

(Cesa et al., 2005; Rossi and Strata, 1995). However, we observed no loss of CF input to *tippy* mutant Purkinje cells but rather an increased density of VGluT2-positive CF terminals studding the dendritic shafts and cell somas of mutant Purkinje cells. Anterogradely labeled CFs twisted up the cell soma and dendritic branches of mutant Purkinje cells with no signs of atrophy, forming active VGluT2-positive synaptic contacts that generated CF-EPSC amplitudes comparable to those in control cerebella. Thus, *tippy* mutant Purkinje cells do not exhibit olivocerebellar input loss. Interestingly, Purkinje cells deprived of PF input, such as in the *weaver* cerebellum, also form a significant number of dendritic spines on first and second order branches (Rakic and Sidman, 1973). Although the decreased PF-EPSC amplitudes in homozygous *tippy* mutant mice imply a reduction in PF-Purkinje cell synapses, we observed an apparently normal PF terminal density based on VGluT1-staining. Further, there is no distal expansion of the CF innervation territory associated with the decreased PF-EPSC amplitudes, which is typically accompanied by expansion of CFs into the distal PF domain of Purkinje cell arbors in other mutants (Takayama et al., 1996; Landsend et al., 1997; Morando et al., 2001; Ichikawa et al., 2002; Hirai et al., 2005; Sotelo, 1990; Cesa and Strata, 2009). Paradoxically, in *tippy* mutant mice, we observed a significant reduction in the CF terminal reach. Lastly, weakening of PF-Purkinje cell synapses typically results in the persistence of multiple CF innervation (Woodward et al., 1974; Crépel, 1982; Mariani, 1982; Scelfo and Strata, 2005; Obtsuki and Hirano, 2008; Hashimoto et al., 2009; Obtsuki et al., 2009). Although there was a trend towards more Purkinje cells maintaining innervation by multiple CFs based on morphological assessment, electrophysiologically, there were no differences in CF:Purkinje cell relationships between wild-type and mutant animals. It is possible that in tippy mutant Purkinje cells, neighboring minor CFs project to Purkinje cellsm but that their function is weak or inactive. Regardless, given that *tippy* mutant cerebella exhibit none of the associated features reported with loss of granule cells or PF input, it is unlikely that the altered spine distribution in mutant mice is a direct consequence of decreased PF-Purkinje cell synaptic contacts.

The tippy degenerative phenotype is unique

Tippy Purkinje cell degeneration affects both the somatodendritic and axonal compartments, with dystrophic alterations, such as axonal torpedos and terminal swellings more numerous than dark axons and dark terminals. These alterations are accompanied by distinct activation of both the astroglial and the microglial cell populations in the cerebellar cortex, the white matter, and the target nuclei of the Purkinje cell axons. The higher frequency of occurrence of dystrophic and overtly degenerative changes in the distal axonal compartment compared to the somatodendritic compartment of the Purkinje cell would seem more compatible with a dying-back form of pathology, rather than with Wallerian degeneration following Purkinje cell death. This brings to mind other neurodegenerative processes described in different mammalian species, including human amyotrophic lateral sclerosis (Résibois and Poncelet, 2004; Fischer et al., 2004; Coleman, 2005; Wishart et al. 2006; Fischer and Glass, 2007; Saxena and Caroni, 2007).

We cannot distinguish whether the degenerative dendritic phenotypes are directly related to the dysmorphic dendritic phenotypes that we see in homozygous *tippy* mutants. Other murine mutants with Purkinje cell degeneration, however, do not share the *tippy* dendritic

abnormalities. Furthermore, we observed numerous mutant Purkinje cells with abnormal dendritic morphology that show no overt signs of distress or degeneration. This observation may imply these phenotypes are separable, or alternatively may indicate that the degenerative process is stochastic within Purkinje cells of abnormal morphology.

Most cerebellar degenerative mutants exhibit rapid apoptotic Purkinje cell death leaving "holes" in the Purkinje cell monolayer. The *tippy* non-apoptotic cell death we have described is apparently a slow process, with little evidence of "missing" Purkinje cells even as late as P35, although our calbindin/VGLUT1 immunostaining suggests the presence of presynaptic PF terminals without postsynaptic Purkinje cell partners. Studies of *staggerer* and *nervous* mutants have shown that just as Purkinje cell dendritic spines form through intrinsic mechanisms that do not depend on axonal synaptic contact, the differentiation and stabilization of presynaptic elements in the PFs may also be driven by a granule cell intrinsic developmental program (Sidman et al., 1962; Sotelo and Changeux, 1974; Herrup, 1983; Doulazmi et al., 2001; Pfenninger et al., 1969; Sotelo, 1973; Landis and Sidman, 1978; Sotelo and Triller, 1979). Therefore, the PF terminals lacking clear associations with any Purkinje cell spines in homozygous *tippy* mutant cerebella may be apposed to calbindin-negative glial processes or they may be devoid of postsynaptic partners. Our electron microscopic examination of *tippy* mutant and control mice did not reveal a widespread presence of naked spines in *tippy* mutant cerebella. However, a definitive test of this hypothesis requires quantitative ultrastructural studies on serial sections from a larger sample to evaluate Purkinje cell-PF synapses as well as any "naked" afferent presynaptic terminals.

The increase in lysosomes and autolysosomes-like bodies, mitochondrial appositions, density of toluidine blue staining and electron microscopic opacity in the affected mutant Purkinje cells suggest a process of activation of autophagy leading to dark cell degeneration (Eskelinen and Saftig, 2009). This type of degeneration is often associated with acute or progressive non-apoptotic (caspase-3 and TUNEL negative) cell death (Yang et al., 2008; Kaja et al., 2011). Furthermore, the large assemblies of dilated and vesiculated endoplasmic reticulum cisterns, which are major sites of dendritic calcium storage, point to severe disturbance of calcium clearance mechanisms that may exacerbate cell stress and cause a toxic cascade (Hoyer-Hansen et al., 2007; Ivannikov et al., 2010).

Overall, the alterations we uncovered in the dendritic and axonal compartments appeared more widespread than the alterations we could detect in the Purkinje cell bodies, suggesting a defect in cell trafficking. The pervasive dystrophy of the Purkinje cell axon terminals in the cerebellar and vestibular nuclei in conjunction with the alterations of PF synapses in the molecular layer are likely to dramatically affect the output of the cerebellum. Many cerebellar mutants such as *pcd* demonstrate ataxia only after more than 50% of Purkinje cells are lost (Mullen et al., 1976). Homozygous *tippy* mutants are ataxic at early postnatal stages without this large scale loss, suggesting that alterations of synaptic activity in the cerebellar and vestibular nuclei engender a circuit pathology well ahead of a definitive cell loss in the cerebellar cortex. We propose, therefore, that the dystrophic changes in the Purkinje cell axons, in combination with abnormalities in the balance and dynamics of CF

and PF excitatory afferent input to the cerebellar cortex, underlie the severe ataxia of *tippy* mutants.

We presume that the severe cerebellar ataxia contributes to the post-natal lethality seen in *tippy* homozygotes, likely compromising the ability of these animals to feed efficiently. In the initial phenotypic report (1995), Lane and Bronson did not report any gross phenotypic brain abnormalities in *tippy* animals. Likewise, our own survey of brain regions did not reveal readily observable phenotypes outside of the cerebellar hypoplasia in other motor regions. Notably we observed subtle structural defects of the hippocampal dentate gyrus in ~10% of animals and this defect may contribute to seizures we have observed in a small subset of animals (data not shown). However, since only a subset of animals are affected, this defect cannot account for the high rate of lethality. Further analysis of other brain regions and cause of death will be greatly facilitated by the characterization of the molecular lesion in *tippy* mutants and knowledge of the affected genes.

The tippy mutant is molecularly unique

Although the causative *tippy* gene has yet to be identified, none of the genes in the refined *tippy* critical region have previously been implicated in ataxia, Purkinje cell development or neuronal degeneration and survival. Thus, the *tippy* mutant embodies a novel cerebellar phenotype centered with a primary defect in Purkinje cells caused by a heretofore unrecognized player in Purkinje cell morphogenesis and homeostasis. The elucidation of the causative *tippy* gene and dissection of its mechanism of action will provide much needed insight into the intrinsic developmental signals that regulate Purkinje cell dendritic development and the establishment of normal cerebellar circuitry.

Supplementary Material

Refer to Web version on PubMed Central for supplementary material.

Acknowledgements

We thank M. Rose Rogers, Nicholas Trojanowski and Paul Wakenight for their invaluable technical assistance. This work was supported by NIH grants R03 NS065382 (KJM), R01 NS050386 and R01 NS072441 (KJM), R01 NS09904 (EM), T32 GM007281 (EKS), NRSA F31NS061436-01 (EKS), with additional funding from NWO-ALW 817.02.013 (CH) and the Brain Research Foundation (KJM).

References

Barclay J, Balaguero N, Mione M, Ackerman SL, Letts VA, Brodbeck J, Canti C, Meir A, Page KM, Kusumi K, Perez-Reyes E, Lander ES, Frankel WN, Gardiner RM, Dolphin AC, Rees M. *Ducky* mouse phenotype of epilepsy and ataxia is associated with mutations in the Cacna2d2 gene and decreased calcium channel current in cerebellar Purkinje cells. J Neurosci. 2001; 21:6095–6104. [PubMed: 11487633]

Cesa R, Morando L, Strata P. Glutamate receptor delta2 subunit in activity-dependent heterologous synaptic competition. J Neurosci. 2003; 23:2363–2370. [PubMed: 12657696]

Cesa R, Morando L, Strata P. Purkinje cell spinogenesis during architectural rewiring in the mature cerebellum. Eur J Neurosci. 2005; 22:579–586. [PubMed: 16101739]

Cesa R, Strata P. Axonal competition in the synaptic wiring of the cerebellar cortex during development and in the mature cerebellum. Neuroscience. 2009; 162:624–632. [PubMed: 19272433]

Chizhikov VV, Millen KJ. Control of roof plate formation by Lmx1a in the developing spinal cord. Development. 2004; 131:2693–2705. [PubMed: 15148302]

Chizhikov VV, Davenport J, Zhang Q, Shih EK, Cabello OA, Fuchs JL, Yoder BK, Millen KJ. Cilia proteins control cerebellar morphogenesis by promoting expansion of the granule progenitor pool. J Neurosci. 2007; 27:9780–9789. [PubMed: 17804638]

Coleman M. Axon degeneration mechanisms: commonality amid diversity. Nat Rev Neurosci. 2005; 6:889–898. [PubMed: 16224497]

Crépel F. Regression of functional synapses in the immature mammalian cerebellum. Trends Neurosci. 1982; 5:266–269.

Crépel F, Delhaye-Bouchaud N, Dupont JL. Fate of the multiple innervation of cerebellar Purkinje cells by climbing fibers in immature control, x-irradiated and hypothyroid rats. Brain Res. 1981; 227:59–71. [PubMed: 7470934]

Doulazmi M, Frederic F, Capone F, Becker-Andre M, Delhaye-Bouchaud N, Mariani J. A comparative study of Purkinje cells in two RORalpha gene mutant mice: staggerer and RORalpha(−/−). Brain Res Dev Brain Res. 2001; 127:165–174. [PubMed: 11335003]

Eskelinen EL, Saftig P. Autophagy: A lysosomal degradation pathway with a central role in health and disease. Biochim Biophys Acta. 2009; 1793:664–673. [PubMed: 18706940]

Faust P. Abnormal cerebellar histogenesis in PEX2 Zellweger mice reflects multiple neuronal defects induced by peroxisome deficiency. J Comp Neurol. 2003; 461:394–3413. [PubMed: 12746876]

Fisher LR, Culver DG, Tennant P, et al. Amyotrophic lateral sclerosis is a distal axonopathy in mice and man. Exp Neurol. 2004; 185:20534–22542.

Fischer LR, Glass JD. Axonal degeneration in motor neuron disease. Neurodegener Dis. 2007; 4:431–442. [PubMed: 17934327]

Grüsser-Cornehls U, Bäurle J. Mutant mice as a model for cerebellar ataxia. Progress in Neurobiology. 2001; 63:489–540. [PubMed: 11164620]

Gudbjartsson DF, Thorvaldsson T, Kong A, Gunnarsson G, Ingolfsdottir A. Allegro version 2. Nat Genet. 2005; 37:1015–1016. [PubMed: 16195711]

Hashimoto K, Yoshida T, Sakimura K, Mishina M, Watanabe M, Kano M. Influence of parallel fiber-Purkinje cell synapse formation on postnatal development of climbing-fiber-Purkinje cell synapses in the cerebellum. Neuroscience. 2009; 162:601–611. [PubMed: 19166909]

Hering H, Sheng M. Dendritic spines: structure, dynamics and regulation. Nat Rev Neurosci. 2001; 2:880–888. [PubMed: 11733795]

Herrup K. Role of staggerer gene in determining cell number in cerebellar cortex. I. Granule cell death is an indirect consequence of staggerer gene action. Brain Res. 1983; 313:267–374. [PubMed: 6667376]

Hirai H, Pang Z, Bao D, Miyazaki T, Li L, Miura E, Parris J, Rong Y, Watanabe M, Yuzaki M, Morgan JI. Cbln1 is essential for synaptic integrity and plasticity in the cerebellum. Nat Neurosci. 2005; 8:1534–1541. [PubMed: 16234806]

Hirano T. Cerebellar regulation mechanisms learned from studies on GluRdelta2. Mol Neurobiol. 2006; 33:1–16. [PubMed: 16388107]

Hoyer-Hansen M, Bastholm l, Szyniarowski P, Campanella M, Szabadkai G, Farkas T, Bianchi K, Fehrenbacher N, Elling F, Rizzuto R, Mathiasen IS, Jäättelä M. Control of macroautophagy by calcium, calmodulin-dependent kinase kinase-β, and Bcl-2. Mol Cell. 2007; 25:193–205. [PubMed: 17244528]

Ichikawa R, Miyazaki T, Kano M, Hashikawa T, Tatsumi H, Sakimura K, Mishina M, Inoue Y, Watanabe M. Distal extension of climbing fiber territory and multiple innervations caused by aberrant wiring to adjacent spiny branchlets in cerebellar Purkinje cells lacking glutamate receptor delta 2. J Neurosci. 2002; 22:8487–8503. [PubMed: 12351723]

Ideraabdullah FY, Kim K, Pomp D, Moran JL, Beier D, Villena FP. Rescue of the Mouse DDK Syndrome by Parent-of-Origin-Dependent Modifiers. Biol Reprod. 2007; 76:286–293. [PubMed: 17050856]

Ivannikov MV, Sugimori M, Llinás R. Calcium clearance and its energy requirements in cerebellar neurons. Cell Calcium. 2010; 47:507–513. [PubMed: 20510449]

Kaja S, Duncan RS, Longoria S, Hilgenberg JD, Payne AJ, Desai NM, Parikh R, Burroughs SL, Gregg EV, Goad DL, Koulen P. Novel mechanism of increased Ca(2+) release following oxidative stress in neuronal cells involves type 2 inositol-1,4,5-trisphosphate receptors. Neuroscience. 2011; 175:281–291. [PubMed: 21075175]

Kapfhammer JP. Cellular and molecular control of dendritic growth and development of cerebellar Purkinje cells. Prog Histochem Cytochem. 2004; 39:131–182. [PubMed: 15580762]

Konnerth A, Llano I, Armstrong CM. Synaptic currents in cerebellar Purkinje cells. Proc Natl Acad Sci U SA. 1990; 87:2662–2665.

Landis DM, Sidman RL. Electron microscopic analysis of postnatal histogenesis in the cerebellar cortex of staggerer mutant mice. J Comp Neurol. 1978; 179:831–863. [PubMed: 641237]

Landsend AS, Amiry-Moghaddam M, Matsubara A, Bergersen L, Usami S, Wenthold RJ, Ottersen OP. Differential localization of delta glutamate receptors in the rat cerebellum: coexpression with AMPA receptors in parallel fiber-spine synapses and absence from climbing fiber-spine synapses. J Neurosci. 1997; 17:834–842. [PubMed: 8987804]

Lane PW, Bronson RT. *Tippy* (tip) A lethal mutation on chromosome 9 in the mouse. Mouse Genome. 1995; 93:158–160.

Larramendi EM, Victor T. Synapses on the Purkinje cell spines in the mouse. An electron microscopic study. Brain Res. 1967; 5:15–30. [PubMed: 6035937]

Llinás R, Sugimori M. Electrophysiological properties of in vitro Purkinje cell dendrites in mammalian cerebellar slices. J Physiol. 1980; 305:197–213. [PubMed: 7441553]

Mariani J. Extent of multiple innervation of Purkinje cells by climbing fibers in the olivocerebellar system of weaver, reeler, and staggerer mutant mice. J Neurobiol. 1982; 13:119–126. [PubMed: 7062017]

Matsubayashi Y, Iwai L, Kawasaki H. Flourescent double-labeling with carbocyanine neuronal tracing and immunohistochemistry using a cholesterol-specific detergent digitonin. J Neurosci Methods. 2008; 174:71–81. [PubMed: 18674563]

Meisler MH, Sprunger LK, Plummer NW, Escayg A, Jones JM. Ion channel mutations in mouse models of inherited neurological disease. Ann Med. 1997; 29:569–574. [PubMed: 9562526]

Moran JL, Bolton AD, Tran PV, Brown A, Dwyer ND, Manning DK, Bjork BC, Li C, Montgomery K, Siepka SM, Vitaterna MH, Takahashi JS, Wiltshire T, Kwiatkowski DJ, Kucherlapati R, Beier DR. Utilization of a whole genome SNP panel for efficient genetic mapping in the mouse. Genome Res. 2006; 16:436–440. [PubMed: 16461637]

Morando L, Cesa R, Rasetti R, Harvey R, Strata P. Role of glutamate delta −2 receptors in activity-dependent competition between heterologous afferent fibers. Proc Natl Acad Sci U SA. 2001; 98:9954–9959.

Mugnaini E, Berrebi AS, Dahl AL, Morgan JI. The polypeptide PEP-19 is a marker for Purkinje neurons in cerebellar cortex and cartwheel neurons in the dorsal cochlear nucleus. Arch Ital Biol. 1987; 126:41–67. [PubMed: 3449006]

Mullen RJ, Eicher EM, Sidman RL. Purkinje cell degeneration, a new neurological mutation in the mouse. Proc Natl Acad Sci USA. 1976; 73:208–212. [PubMed: 1061118]

Ohtsuki G, Piochon C, Hansel C. Climbing fiber signaling and cerebellar gain control. Front Cell Neurosci. 2009; 3:4. eCollection 2009. [PubMed: 19597563]

Ohtsuki G, Hirano T. Bidirectional plasticity at developing climbing fiber-Purkinje neuron synapses. Eur J Neurosci. 2008; 28:2393–2400. [PubMed: 19032589]

Palay, SL.; Chan-Palay, V. Cerebellar Cortex. New York: Springer-Verlag; 1974.

Perkel DJ, Hestrin S, Sah P, Nicoll RA. Excitatory synaptic currents in Purkinje cells. Proc Biol Sci. 1990; 241:116–121. [PubMed: 1978337]

Pfenninger K, Sandri C, Akert K, Eugster CH. Contribution to the problem of structural organization of the presynaptic area. Brain Res. 1969; 12:10–18. [PubMed: 4184686]

Rakic P, Sidman RL. Organization of cerebellar cortex secondary to deficit of granule cells in weaver mutant mice. J Comp Neurol. 1973; 152:133–161. [PubMed: 4761656]

Résibois A, Poncelet L. Purkinje cell neuroaxinal dystrophy similar to nervous mutant mice phenotype in two sibling kittens. Acta Neuropathol. 2004; 107:553–558. [PubMed: 15042386]

Rossi F, Strata P. Reciprocal trophic interactions in the adult climbing fibre-Purkinje cell system. Prog Neurobiol. 1995; 47:341–369. [PubMed: 8966210]

Rossi F, van der Want JJ, Wiklund L, Strata P. Reinnervation of cerebellar Purkinje cells by climbing fibres surviving a subtotal lesion of the inferior olive in the adult rat. II. Synaptic organization on reinnervated Purkinje cells. J Comp Neurol. 1991; 308:536–554. [PubMed: 1865016]

Sarna JR, Hawkes R. Patterned Purkinje cell death in the cerebellum. Prog Neurobiol. 2003; 70:473–507. [PubMed: 14568361]

Saxena S, Caroni P. Mechanisms of axon degeneration: from development to disease. Prog Neurobiol. 2007; 83:174–191. [PubMed: 17822833]

Scelfo B, Strata P. Correlation between multiple climbing fibre regression and parallel fibre response development in the postnatal mouse cerebellum. Eur J Neurosci. 2005; 21:971–978. [PubMed: 15787703]

Schmued LC, Stowers CC, Scallet AC, Xu L. Fluoro-Jade C results in ultra high resolution and contrast labeling of degenerating neurons. Brain Res. 2005; 1035:24–31. [PubMed: 15713273]

Sekerková G, Diño MR, Ilijic E, Russo M, Zheng L, Bartles JR, Mugnaini E. Postsynaptic enrichment of Eps8 at dendritic shaft synapses of unipolar brush cells in rat cerebellum. Neuroscience. 2007; 145:116–129. [PubMed: 17223277]

Sidman RL, Lane PW, Dickie MM. Staggerer, a new mutation in the mouse affecting the cerebellum. Science. 1962; 137:610–612. [PubMed: 13912552]

Sidman RL, Appel SH, Fullier JF. Neurological mutants of the mouse. Science. 1965; 150:513–516. [PubMed: 17842761]

Sotelo C. Permanence and fate of paramembranous synaptic specializations in "mutants" experimental animals. Brain Res. 1973; 62:345–351. [PubMed: 4760511]

Sotelo C. Anatomical, physiological and biochemical studies of the cerebellum from mutant mice. II. Morphological study of cerebellar cortical neurons and circuits in the weaver mouse. Brain Res. 1975; 94:19–44. [PubMed: 1148865]

Sotelo C, Changeux JP. Transsynaptic degeneration 'en cascade' in the cerebellar cortex of staggerer mutant mice. Brain Res. 1974; 67:519–526. [PubMed: 4470439]

Sotelo C, Triller A. Fate of presynaptic afferents to Purkinje cells in the adult nervous mutant mouse: a model to study presynaptic stabilization. Brain Res. 1979; 175:11–36. [PubMed: 487138]

Sotelo C, Alvarado-Mallart RM. Reconstruction of the defective cerebellar circuitry in adult Purkinje cell degeneration mutant mice by Purkinje cell replacement through transplantation of solid embryonic implants. Neuroscience. 1987; 20:1–22. [PubMed: 3561760]

Sotelo C, Arsenio-Nunes ML. Development of Purkinje cells in absence of climbing fibers. Brain Res. 1976; 111:289–295. [PubMed: 949602]

Sotelo C, Hillman DE, Zamora AJ, Llinas R. Climbing fiber deafferentation: its action on Purkinje cell dendritic spines. Brain Res. 1975; 98:574–581. [PubMed: 1182538]

Takayama C, Nakagawa S, Watanabe M, Mishina M, Inoue Y. Developmental changes in expression and distribution of the glutamate receptor channel delta 2 subunit according to the Purkinje cell maturation. Brain Res Dev Brain Res. 1996; 92:147–155. [PubMed: 8738121]

Wishart TM, Parson SH, Gillingwater TH. Synaptic vulnerability in neurodegenerative disease. J Neuropathol Exp Neurol. 2006; 65:733–739. [PubMed: 16896307]

Woodward DJ, Hoffer BJ, Altman J. Physiological and pharmacological properties of Purkinje cells in rat cerebellum degranulated by postnatal x-irradiation. J Neurobiol. 1974; 5:283–304. [PubMed: 4155719]

Yang DS, Kumar A, Stavrides P, Peterson J, Peterhoff CM, Pawlik M, Levy E, Cataldo AM, Nixon RA. Neuronal apoptosis and autophagy cross talk in aging PS/APP mice, a model of Alzheimer's disease. Am J Pathol. 2008; 173:665–681. [PubMed: 18688038]

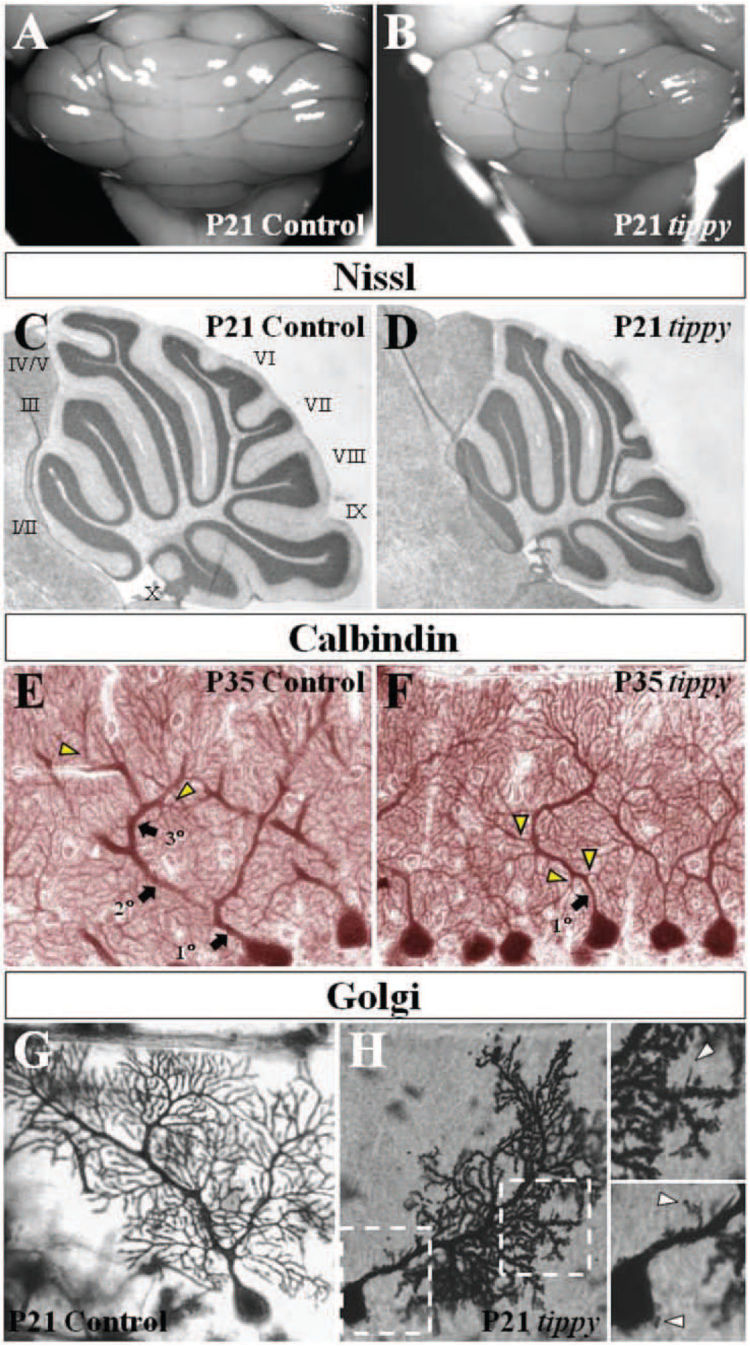

Figure 1. Abnormal mutant Purkinje cells without gross cerebellar dysmorphology in homozygous *tippy* mutant mice

A,B, Whole cerebella of *tippy* mutant mice (***B***) exhibit grossly normal morphology with no significant differences from control cerebella (***A***). The midline structure in (B) is a prominent blood vessel in this particular specimen, a feature that is variable in both wild-type and mutant animals. There is no evidence of aberrant foliation or midline fusion deficits in tippy animals. ***C,D,*** Nissl stained mid-sagittal sections similarly demonstrate normal foliation pattern and cortical laminar structure in mutant (***D***) and control (***C***) mice. Numeric

assignments for the lobules are shown for the control mice (***C***). ***E,F,*** Calbindin stained sagittal sections of cerebella from control (***E***) and *tippy* mutants (***F***) illustrate a dendritic branching malformation in mutant mice. In contrast to the stereotypical hierarchical Purkinje cell branching pattern displayed in control mice with spiny branchlets emerging only from tertiary branches (***E***, arrowheads), *tippy* mutant Purkinje cells display no clear secondary or tertiary shaft dendrites and spiny branchlets emerge directly from the primary dendrite (***F***, arrowheads). ***G,H,*** Golgi-stained Purkinje cells of control (***G***) and *tippy* mutant mice (***H***) reveal a loss of parasagittal planarity as well as a dendritic spine malformation with dendritic spines of immature morphology abnormally studding the proximal dendrite (***H***, top inset, arrowhead) and soma (***H***, bottom inset, arrowheads) in the mutant. Left and right boxed areas are shown at higher magnification as bottom and top insets, respectively.

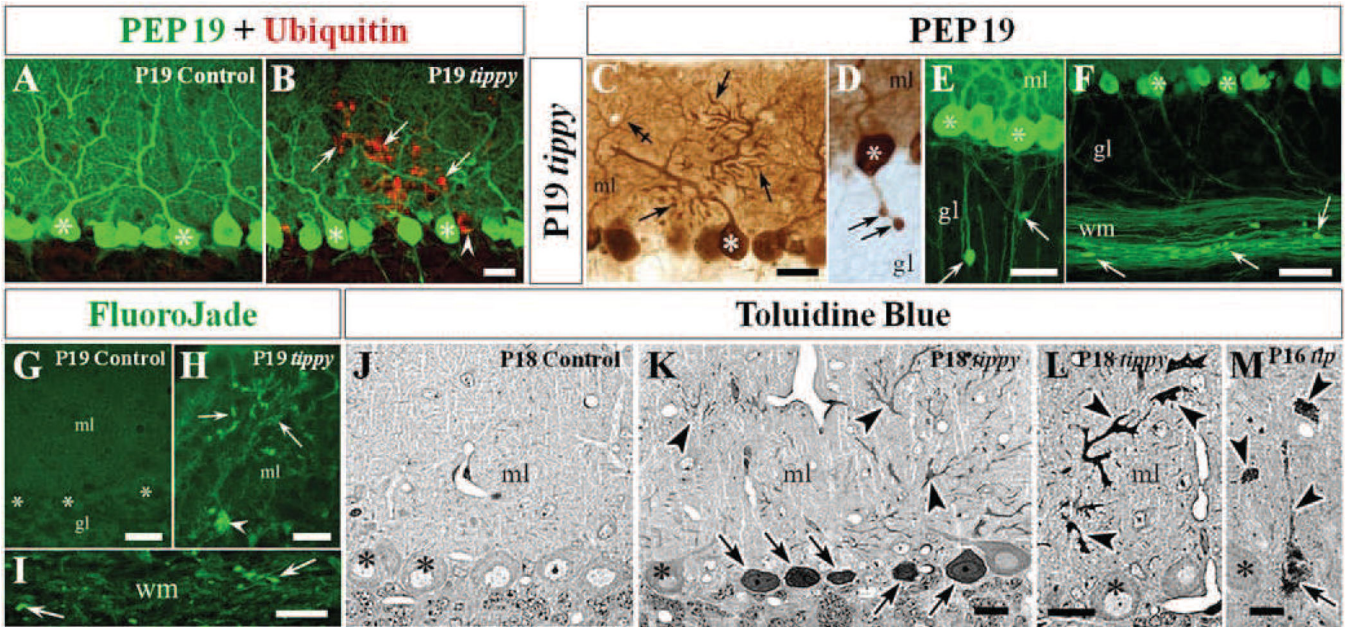

Figure 2. Purkinje cell degeneration in homozygous *tippy* mutant mice cerebella

A,B, Control (***A***) and *tippy* mutant (***B***) mice cerebella stained with PEP19 (green) and ubiquitin (red) demonstrate ubiquitin-positive degenerating Purkinje cell somas (**B**, arrowhead) and degenerating dendritic arbors (**B**, arrows) in *tippy* mutant mice while there is no ubiquitin signal in control Purkinje cells (***A***). ***C–F,*** PEP19 immunostaining further reveals *tippy* mutant Purkinje cells with dysmorphic, degenerating spiny branchlets (***C***, arrows) and axonal spheroids (torpedoes) in the initial axonal segment (***D***, arrows) as well axonal spheroids in the deep granular layer (***E***, arrows) and white matter (***F***, arrows) of mutant cerebella indicating whole-cell degeneration. Crossed-arrow in panel (***C***) points to the arbor of a neighboring, normal Purkinje cell. ***G–I,*** Fluro-Jade C stained sections demonstrate degenerating Purkinje cell bodies (***H***, arrowhead), dendrites (***H***, arrows) and several white matter axons (***I***, arrows) in *tippy* mutant cerebella but no degeneration signal in the cerebellar cortex of control mice (***G***). ***J–M,*** Semithin (1–2 μm) resin sections stained with toluidine blue illustrate delicately stained Purkinje cells of normal morphology, with the nucleolus being the only dense organelle in control cerebella (***J***). In contrast, *tippy* mutant cerebella demonstrate multiple densely stained Purkinje cell somata (***K,M*** arrows) and severely dysmorphic dendritic arbors (***K–M***, arrowheads) in varying stages of dark degeneration. Asterisks indicate Purkinje cell somas. ml, molecular layer; gl, granule cell layer; wm, white matter. Scale bars: ***A–E, H, J–L,*** 20 μm; ***F, G, I,*** 30 μm; ***M,*** 10 μm (scale bar in ***B, E,*** and ***K*** applies to ***A, D,*** and ***J***, respectively).

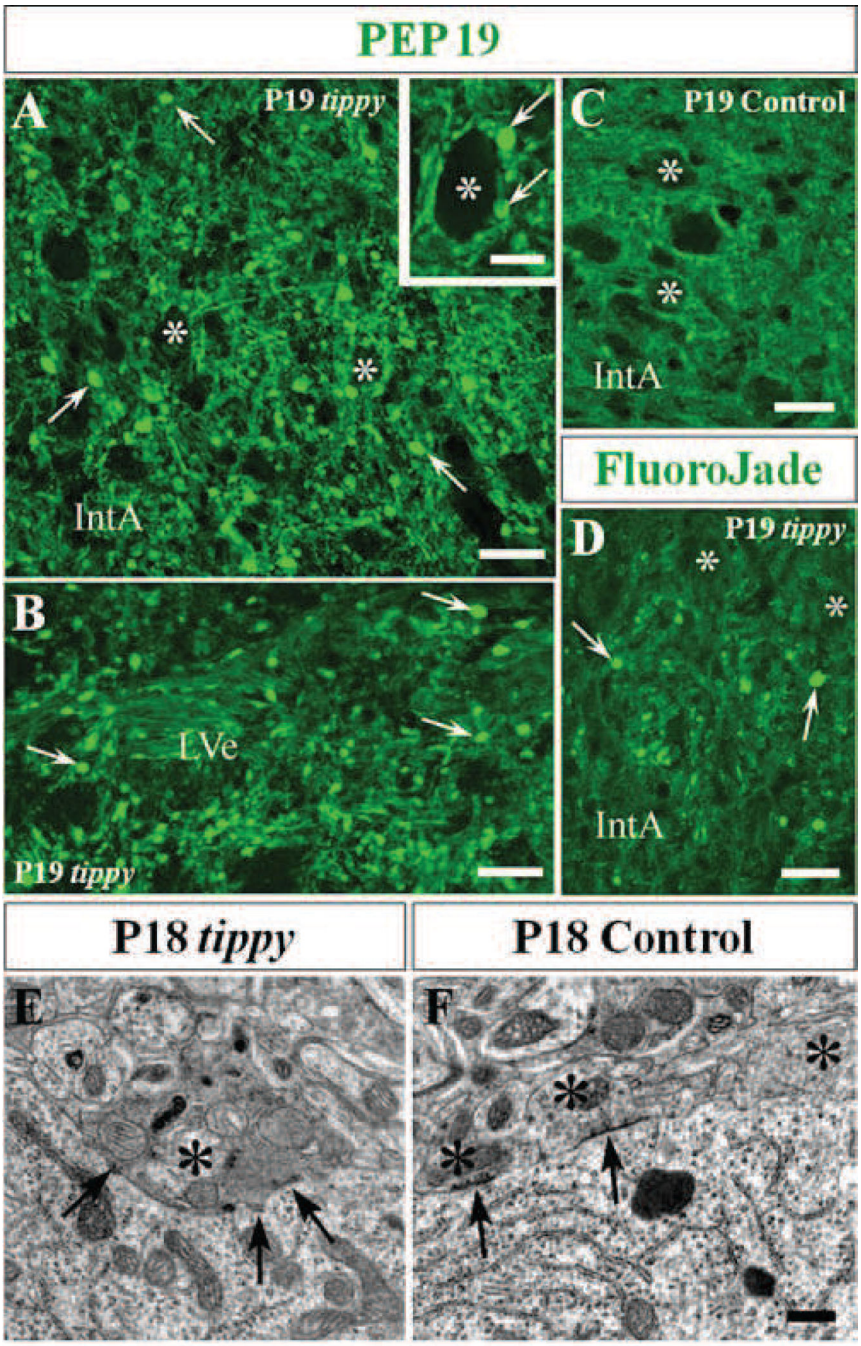

Figure 3. Degenerating Purkinje cell axons and terminals in cerebellar and vestibular nuclei of homozygous *tippy* mutant cerebella

A–D, *Tippy* mutant cerebellar sections demonstrate abundant axonal spheroids (***A,B,D,*** arrows) in the nucleus interpositus anterior (IntA) and the lateral vestibular nucleus (LVe) after staining with PEP 19 (***A,B***) or Fluoro-Jade C (***D***) while there are no spheroids present in the IntA of control cerebella (***C***). PEP19-positive spheroids (arrows) are apposed to the cell body of a large efferent neuron (asterisks) in the medial cerebellar nucleus (***A***, inset). ***E,F,*** Electromicrographs of Purkinje cell terminals in LVe of *tippy* mutant (***E***) and control

(***F***) mice illustrate that the cell body of a normal, large efferent neuron in the LVe of control mice is surrounded by normal Purkinje axon terminals (***F,*** asterisks), three of which contain dispersed small mitrochondia and pleomorphic synaptic vesicles. In contrast, the cell body of a large efferent neuron in the LVe of mutant mice is directly apposed by a swollen dystrophic terminal of a Purkinje cell axon (***E***, asterisk). The organelles in the dystrophic terminal closely resemble those observed in the terminal of the recurrent collateral in the cortex shown in Fig. 4*F*. Arrows indicate symmetric axo-somatic synapses. Scale bars: ***A–D***, 20 μm; ***inset in A***, 10 μm; ***E, F***, 0.5 μm.

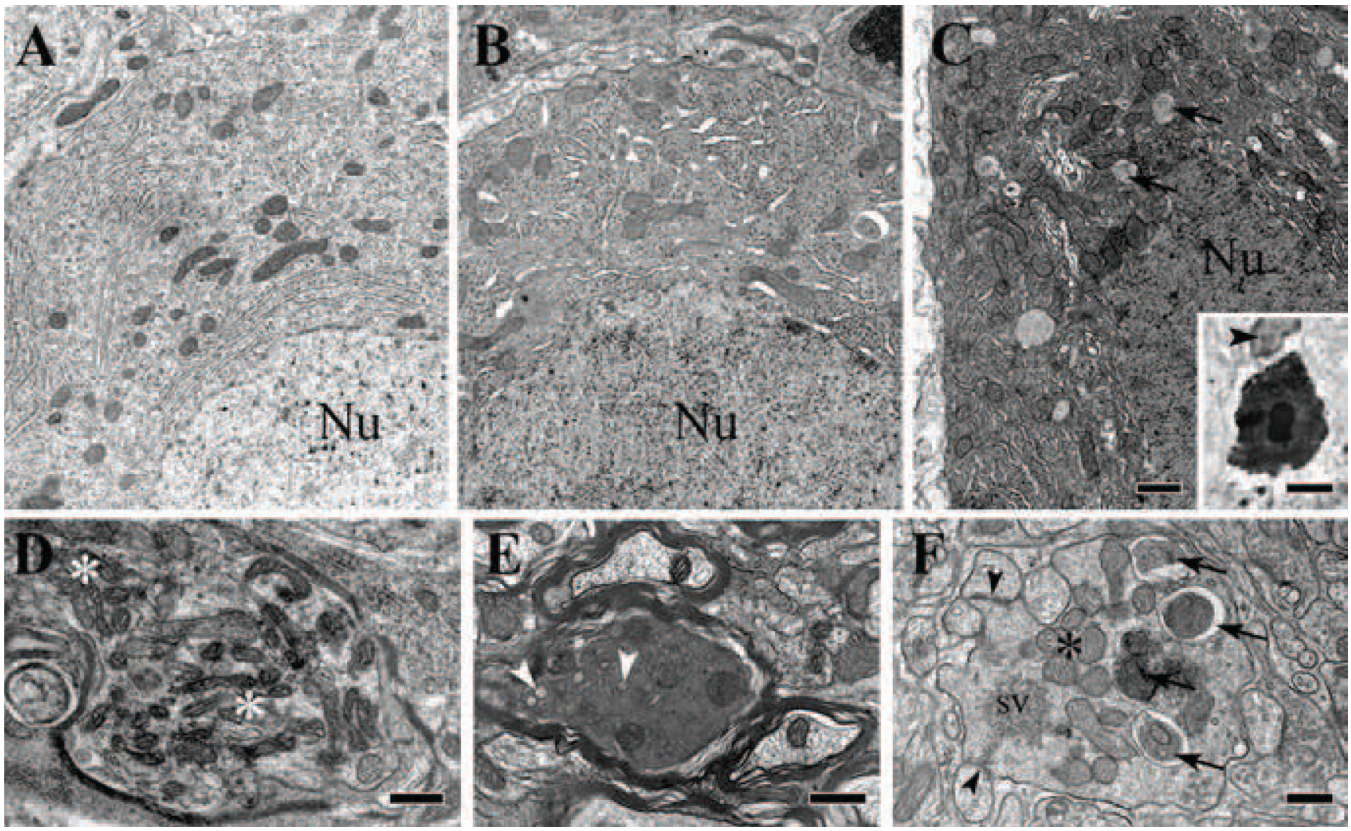

Figure 4. Electron microscopy of normal and degenerating Purkinje cell bodies and axons in P18 homozygous *tippy* mutant mice

A–C, Illustration of the normal appearance of a Purkinje cell body (***A***), a dystrophic cell body with enlarged ER and an autophagosome (***B***), and a shrunken cell body in advanced stage of degeneration showing increased electron density of the cytoplasm, nucleoplasm and nuclear bodies, and a remarkable increase in lysosome-like and autophagosome-like bodies (***C***, arrows). A microglial phagocyte (arrowhead) approaching a shrunken, degenerated Purkinje cell body (***C,*** inset) that is already surrounded by dilated Bergmann glial profiles (unlabeled white halo). ***D,*** A Purkinje cell axon forms a spheroid near the Ranvier heminode and contains clumped mitochondria (asterisks) interspersed with ER vesicles and small autophagosome-like bodies. ***E,*** A Purkinje cell axon in the folial white matter is undergoing dark degeneration. Arrowheads indicate vesiculated ER. ***F,*** A swollen terminal of a Purkinje cell recurrent axon collateral in the molecular layer shows advanced dystrophic signs, as indicated by assembled mitochondria (asterisk), autophagosomes (arrows), and clumped pleomorphic synaptic vesicles (sv). The degenerating profile forms symmetric junctions with Purkinje cell spines (arrowheads). Nu, cell nucleus; sv, synaptic vesicles. Scale bars: ***A–C***, 1 μm; ***inset in C***, 5 μm; ***D–F***, 0.5 μm.

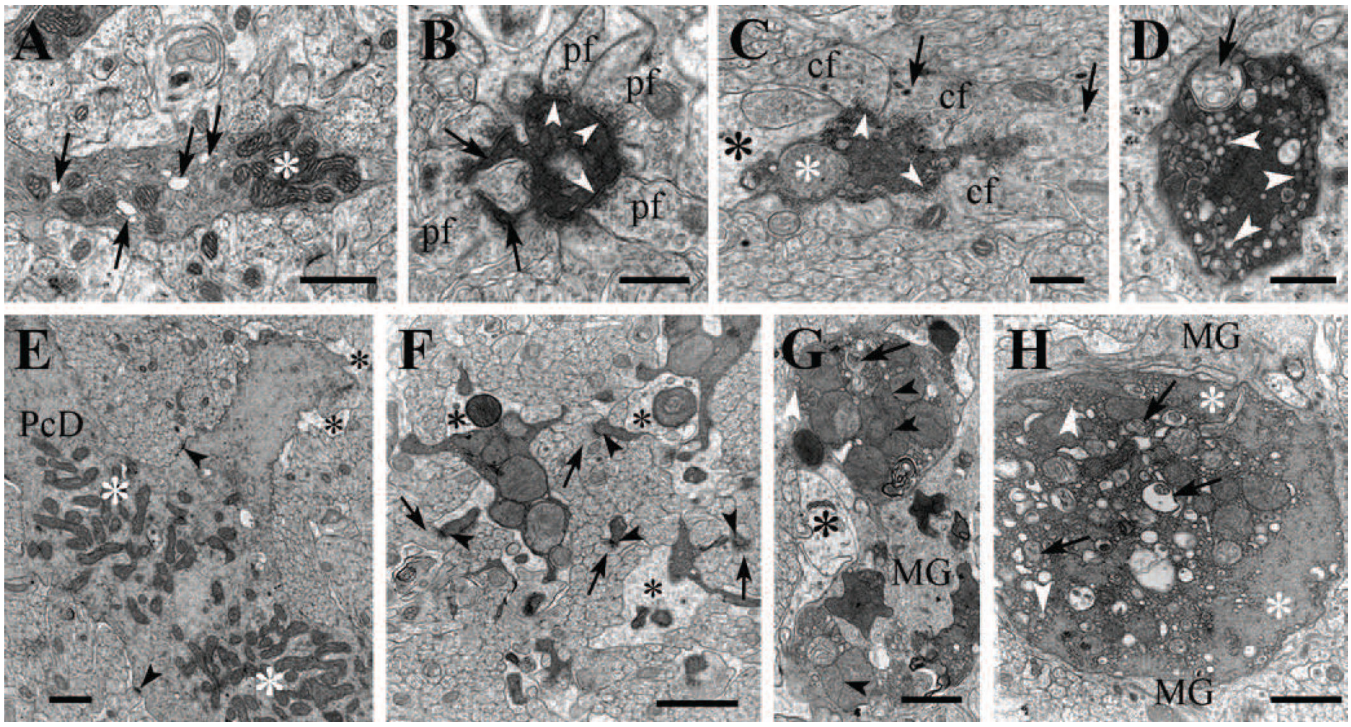

Figure 5. Electron microscopy of degenerating Purkinje cell dendrites in P19 homozygous *tippy* mutant mice

A, A dendritic spiny branchlet contains moderately electron dense cytoplasm, abnormal dilated endoplasmic reticulum (arrows) and clumped mitochondria (asterisk). ***B,*** A degenerating spiny branchlet is surrounded by parallel fiber (PF) varicosities and appears shrunken. Two of its spine synapses (arrows) are still recognizable and PF synapses (arrowheads) are also present on the shaft, possibly corresponding to retracted spines. ***C,*** A degenerating medium-sized dendritic branch appears shrunken, contains an enlarged mitochondrion (white asterisk), is partially surrounded by dilated Bergmann glial processes (black asterisk) and forms synaptic junctions (arrowheads) with climbing fiber varicosities (CF) containing large dense core vesicles (arrows). ***D,*** An overtly degenerating second or third order Purkinje cell dendrite contains double membrane-bound, autophagosome-like bodies (arrow) and clusters of dilated or vesiculated ER cisterns (arrowheads). ***E***, The main stem of a Purkinje cell dendrite (PcD) appears to undergo the initial stage of degeneration; the mitochondria—no longer separated by neurofilaments and microtubules—have formed two large assemblies (white asterisks); some of the ER cisterns appear dilated and the surrounding Bergmann glia profiles are swollen (black asterisk). Arrowheads point to synapses on the dendritic stem. ***F,*** Segmented Purkinje cell branchlets undergoing dark degeneration, are provided with spines (arrowheads) synapsing with parallel fibers (arrows). The branchlets contain small and compact clumps of enlarged mitochondria and are nearly encircled by dilated Bergmann glial processes (asterisks). ***G,H,*** Second and first order branches of a Purkinje cell dendrite undergoing dark degeneration contain enlarged mitochondria and autophagosome-like bodies, and are engulfed by Bergmann glial (black asterisk) and microglial (MG) cell processes. Cisterns of the endoplasmic reticulum (white arrowheads) have become vesiculated and centralized, separating from cytoskeletal elements

(white asterisks). The mitochondrial matrix show varying density. Arrowheads indicate mitochodrial appositions and arrows point to autophagosomes. pf, parallel fiber; cf, climbing fiber; PcD, Purkinje cell dendrite; MG, microglia. Scale bars: ***A, E, G, H***, 1 μm; ***B–D, F***, 0.4 μm.

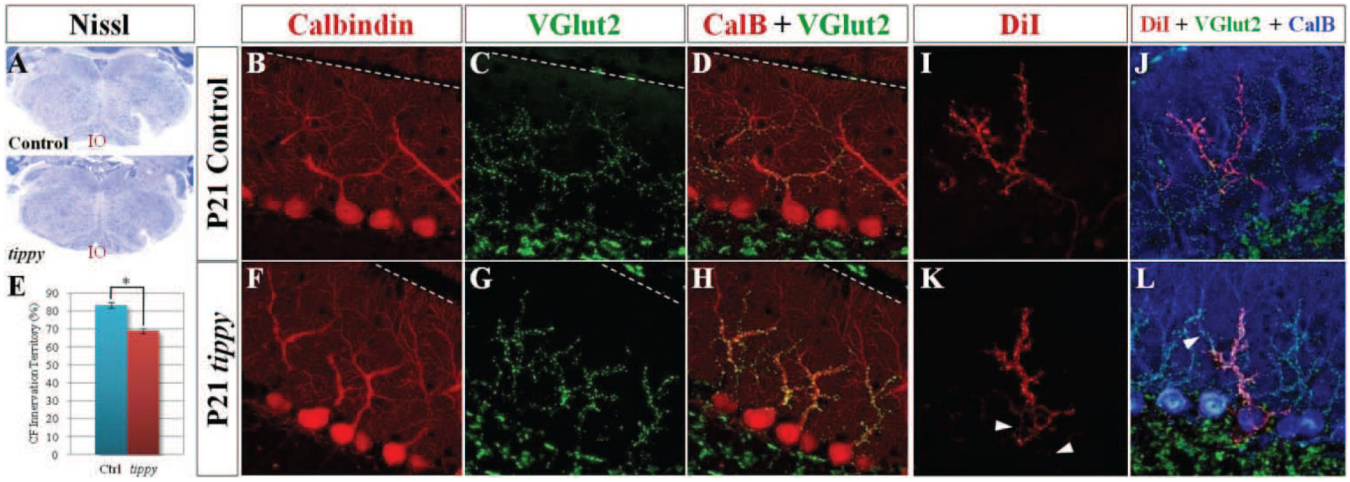

Figure 6. Increased climbing fiber terminals within a reduced dendritic domain and altered pattern of innervation in homozygous *tippy* mutant cerebella

A, Nissl stained coronal sections demonstrate qualitatively normal inferior olivary neurons (IO) in both control and *tippy* mutant mice. ***B–L,*** However, confocal imaged sagittal sections of control (***B–D***) and *tippy* mutant (***F–H***) cerebella stained with calbindin (red; ***B,F***) and VGluT2 (green; ***C,G***) illustrate marked clustering of VGluT2-positive climbing fiber (CF) terminals (***G***) and increased density of CF terminals on the proximal dendrite and soma of *tippy* mutant PCs (***H***) compared to control (***D***). Quantitative analysis of CF innervation territory in P21 mice indicates a significant reduction in the domain encompassed by CF terminals in mutant mice compared to controls (***E***). $n = 10$ for WT, $n = 11$ for mutants. Further, confocal imaged sagittal sections of anterogradely DiI-labeled CFs (red), VGluT2-labeled CF terminals (green) and calbindin-labeled PCs (blue) in control (**J**) and *tippy* mutant (***L***) mice illustrate alterations in the pattern of CF innervation in mutant cerebella. Unlike single DiI-labeled CFs in control mice that travel a direct route to PCs (***I***), DiI-labeled CFs in the mutant cerebellum travel a circuitous path, intertwining with other DiI-labeled CFs in the PC layer (***K***, arrowheads). Triple-labeled images (***J,L***) highlight the increased thickness of CFs in the mutant, presence of DiI-labeled, VGluT2-positive puncta on the mutant PC soma and proximal dendritic shaft as well as the presence of of VGluT2-positive, DiIunlabeled terminals on the same PC (***L***, arrowhead) as VGluT2-positive, DiI-labeled puncta, suggesting multiple innervation. Data are expressed as mean ± SEM. $*p < 0.00001$, Student's *t*-test. The pial surface is indicated by the dotted line.

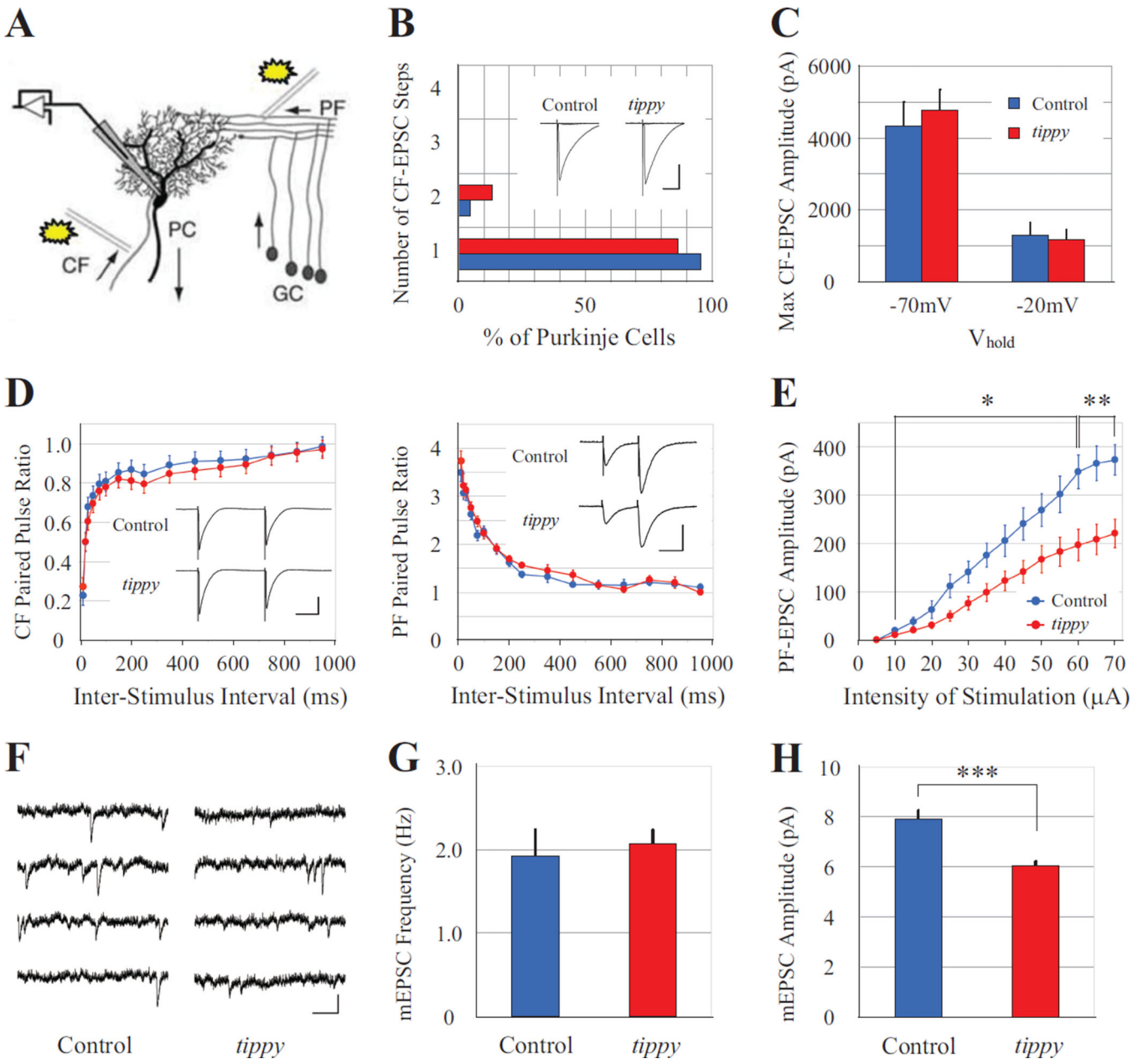

Figure 7. Normal CF-EPSC but reduced PF-EPSC amplitudes in *tippy* mutant mice

A, PCs were whole-cell voltage clamped by a patch electrode with stimulation given to parallel fibers (PFs) or climbing fibers (CFs). ***B,C,*** Histogram of discrete steps of CF-EPSCs in PCs from control (*n* = 22 cells, blue) and *tippy* mutant (*n* = 15 cells, red) mice at P21–P24 (***B***) to assess mono- or multiple CF innervation, demonstrated no significant differences between the genotypes. Typical superimposed CF-EPSC traces at −20 mV are shown in the inset. Scale is 20 ms and 500 pA. CF-EPSCs recorded with membrane potentials held at −70 mV or −20 mV (***C***) indicated no significant difference in the amplitudes between control (*n* = 7 cells, blue) and mutant (n = 6 cells, red) mice at either potential. ***D–E,*** Both CF-EPSCs and PF-EPSCs exhibited normal paired-pulse depression and paired-pulse facilitation (***D***) in control (blue circles) and *tippy* mutant (red circles) mice. Typical CF- and PF-EPSC traces

are shown in insets. CF-EPSC traces at −20 mV. Scale is 50 ms and 500 pA in CF-EPSCs, and 50 ms and 200 pA in PF-EPSCs, respectively. However, PF-EPSCs elicited from control (n = 13 cells, blue) and *tippy* mutant (n = 19 cells, red) PCs demonstrated significantly decreased amplitudes in mutants in response to increasing stimulus intensities (***E***). mEPSCS were recorded from PCs under the bath application of TTX. ***F,*** Representative recordings from control (n = 17 cells) and *tippy* mutant (n = 21 cells) cerebella are shown. Scale is 250 ms and 10 pA. ***G,*** No significant difference was observed in the frequency of mEPSCs between control and mutant mice. ***H,*** However, *tippy* mutant mice exhibited significantly reduced mEPSC amplitudes compared to controls. Data are expressed as mean ± SEM. *p < 0.05; **p < 0.005; ***p < 0.0001, Student's t-test.

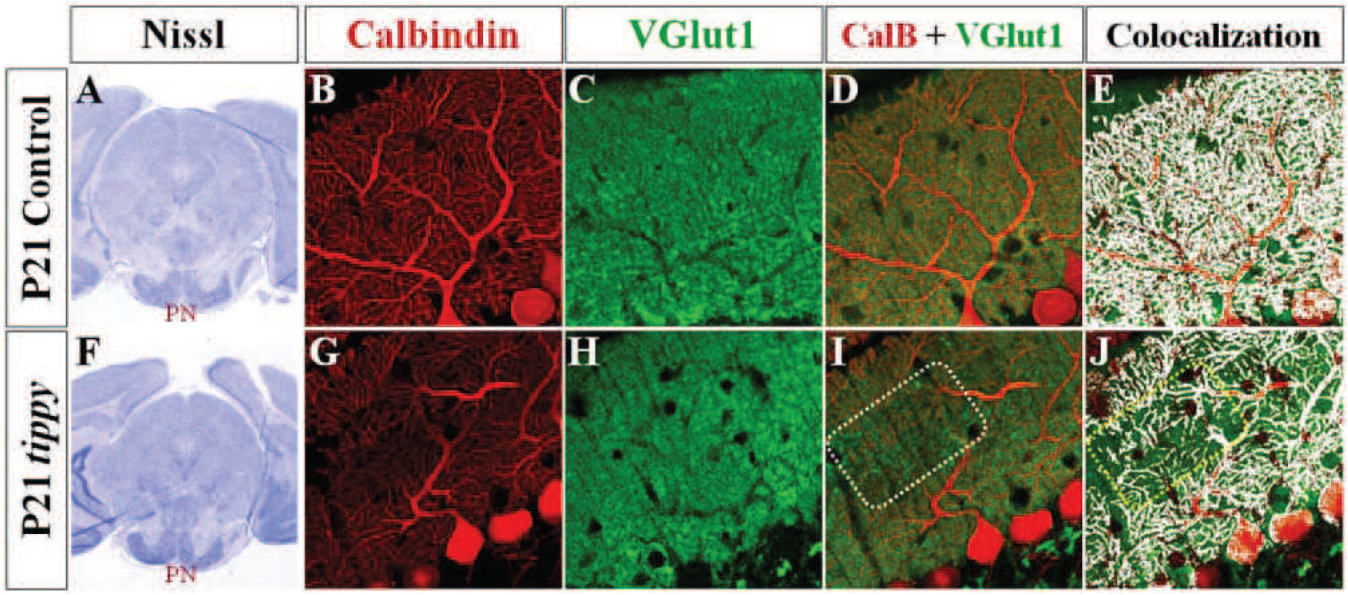

Figure 8. Decreased PF-PC synaptic contacts in homozygous *tippy* mutant mice

A,F, Nissl stained coronal sections demonstrate qualitatively normal pontine nuclei in control (***A***) and *tippy* mutant (***F***) mice at P21. ***B–J,*** Confocal imaged sagittal sections stained with calbindin (red; ***B,G***) and VGluT1 (green; ***C,H***) likewise illustrate VGluT1-positive PF terminals in *tippy* mutant mice (***H***) distributed within an innervation domain and at density comparable to that seen in control cerebella (***C***). However, in contrast to the homogenous overlay between calbindin-labeled PC processes and VGluT1-labeled PF terminals seen in control mice (***D,E***), patches of PF terminals are seen without associated PC processes (***I,J*** boxed regions) in *tippy* mutants. Colocalization of calbindin and VGluT1-labeled puncta are shown in white in (***E,J***).

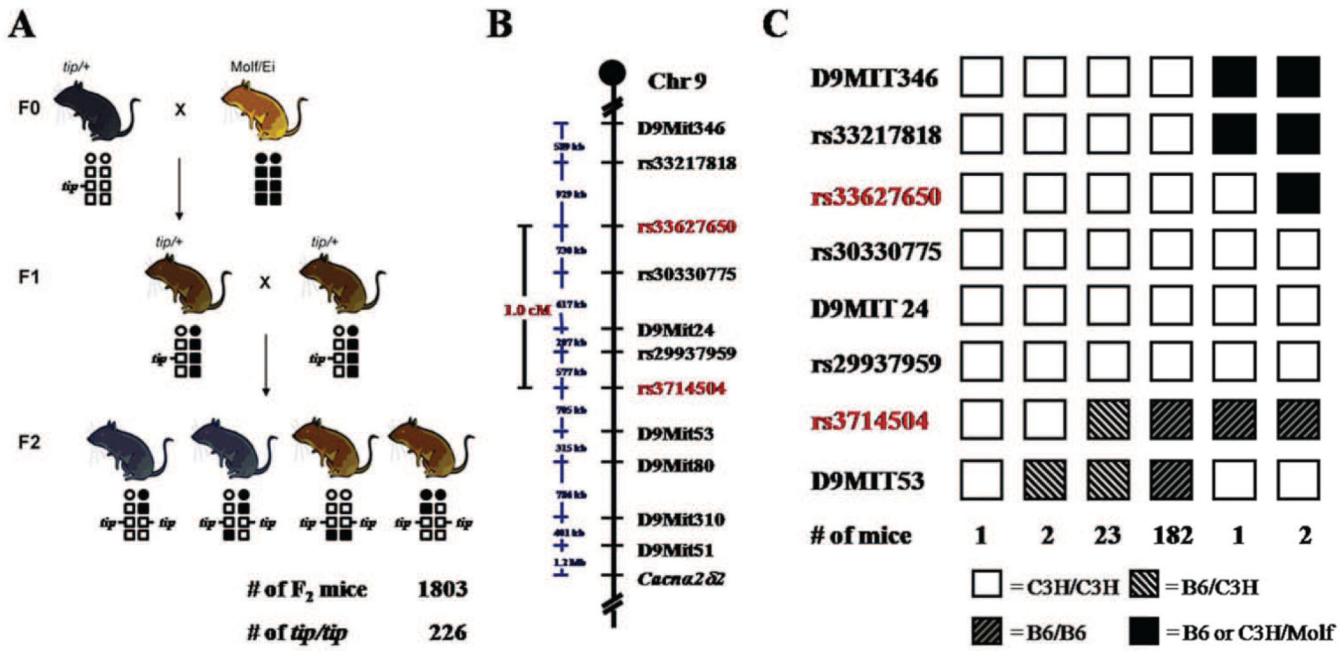

Figure 9. Genetic mapping of the *tippy* locus

A–C, To ascertain the *tippy* gene, an intersubspecific intercross between *tip*/+ heterozygous mice and Molf/E_i mice was performed (***A***). DNA from affected F_2 mice was typed for polymorphic markers, localizing the *tippy* locus to a 1.0 cM/2.1 Mb region on distal chromosome 9 between SNP markers rs33627650 and rs3714504 (***B***, labeled in red). Haplotype analysis of 211 affected F_2 mice defining the maximal critical interval harboring the *tippy* gene on chromosome 9 (***C***). Haplotypes for each marker are shown as columns with numbers of mice represented underneath. White boxes indicate C3H homozygous loci, white striped boxes indicate B6/C3H heterozygous loci, black striped boxes indicate B6 homozygous loci, and black boxes denote C3H or B6/Molf heterozygous loci.